Time-Critical Cooperative Path Following of Multiple UAVs over Time-Varying Networks*

E. Xargay † I. Kaminer ‡ A. Pascoal § N. Hovakimyan ¶ V. Dobrokhodov ‖
V. Cichella ** A. Aguiar †† R. Ghabcheloo ‡‡

This paper addresses the problem of steering a fleet of UAVs along desired paths while meeting stringent spatial and temporal constraints. A representative example is the challenging mission scenario where the vehicles are tasked to cooperatively execute collision-free maneuvers and arrive at their final destinations at the same time (time-critical operations).

In the setup adopted, the vehicles are assigned nominal spatial paths and speed profiles along those. The paths are then appropriately parameterized and the vehicles are requested to execute cooperative path following, rather than "open loop" trajectory tracking maneuvers. This strategy yields robust behavior against external disturbances by allowing the vehicles to negotiate their speeds along the paths in response to information exchanged over the dynamic inter-vehicle communications network.

The paper addresses explicitly the situation where each vehicle transmits its coordination information to only a subset of the other vehicles, as determined by the communications topology. Furthermore, we consider the case where the communications graph that captures the underlying communications topology is disconnected during some interval of time or even fails to be connected at all times. Conditions are given under which the complete time-critical cooperative path-following closed-loop system is stable and yields convergence of a conveniently defined cooperation error to a neighborhood of the origin. Flight test results of a coordinated road search mission demonstrate the efficacy of the multi-UAV cooperative control framework developed in the paper.

I. Introduction

Unmanned Aerial Vehicles (UAVs) are becoming ubiquitous and have been playing an increasingly important role in military reconnaissance and strike operations, border patrol missions, forest fire detection, police surveillance, and recovery operations, to name but a few. In simple applications, a single autonomous vehicle can be managed by a crew using a ground station provided by the vehicle manufacturer. The execution of more challenging missions, however, requires the use of multiple vehicles working in cooperation

*Research supported in part by projects CO3AUVs-IST of the CEC, NAV-Control / FCT-PT (PTDC/EEA-ACR/65996/2006), the FCT-ISR/IST pluriannual funding program through the POS_C Program that includes FEDER funds, USSOCOM, ONR under Contract N00014-05-1-0828, AFOSR under Contract No. FA9550-05-1-0157, and ARO under Contract No. W911NF-06-1-0330.

†PhD Candidate, Department of Mechanical Science & Engineering, University of Illinois at Urbana-Champaign; xargay@illinois.edu.

‡Professor, Department of Mechanical & Astronautical Engineering, Naval Postgraduate School; kaminer@nps.edu.

§Associate Professor, Laboratory of Robotics and Systems in Engineering and Science (LARSyS), Instituto Superior Técnico (IST), Technical University of Lisbon, Portugal; antonio@isr.ist.utl.pt.

¶Professor, Department of Mechanical Science & Engineering, University of Illinois at Urbana-Champaign; nhovakim@illinois.edu.

‖Research Assistant Professor, Department of Mechanical & Astronautical Engineering, Naval Postgraduate School; vldobr@nps.edu.

**Research Associate, Department of Mechanical & Astronautical Engineering, Naval Postgraduate School; venanzio.cichella@gmail.com.

††Assistant Professor, Laboratory of Robotics and Systems in Engineering and Science (LARSyS), Instituto Superior Técnico (IST), Technical University of Lisbon, Portugal; pedro@isr.ist.utl.pt.

‡‡Senior Researcher, Department of Intelligent Hydraulics and Automation, Tampere University of Technology, Finland; reza.ghabcheloo@tut.fi

Report Documentation Page

Form Approved
OMB No. 0704-0188

1. REPORT DATE	2. REPORT TYPE	3. DATES COVERED
2011		**00-00-2011 to 00-00-2011**

4. TITLE AND SUBTITLE	5a. CONTRACT NUMBER
Time-Critical Cooperative Path Following of Multiple UAVs over Time-Varying Networks	5b. GRANT NUMBER
	5c. PROGRAM ELEMENT NUMBER
6. AUTHOR(S)	5d. PROJECT NUMBER
	5e. TASK NUMBER
	5f. WORK UNIT NUMBER
7. PERFORMING ORGANIZATION NAME(S) AND ADDRESS(ES) **Naval Postgraduate School,Department of Mechanical & Astronautical Engineering,Monterey,CA,93943**	8. PERFORMING ORGANIZATION REPORT NUMBER
9. SPONSORING/MONITORING AGENCY NAME(S) AND ADDRESS(ES)	10. SPONSOR/MONITOR'S ACRONYM(S)
	11. SPONSOR/MONITOR'S REPORT NUMBER(S)

12. DISTRIBUTION/AVAILABILITY STATEMENT
Approved for public release; distribution unlimited

13. SUPPLEMENTARY NOTES
submitted to AIAA Journal of Guidance, Control and Dynamics

14. ABSTRACT

15. SUBJECT TERMS

16. SECURITY CLASSIFICATION OF:			17. LIMITATION OF ABSTRACT	18. NUMBER OF PAGES	19a. NAME OF RESPONSIBLE PERSON
a. REPORT **unclassified**	b. ABSTRACT **unclassified**	c. THIS PAGE **unclassified**	**Same as Report (SAR)**	**36**	

to achieve a common objective. Representative examples of cooperative mission scenarios are sequential auto-landing and coordinated ground target suppression for multiple UAVs. The first refers to the situation where a fleet of UAVs must break up and arrive at the assigned glideslope point, separated by pre-specified safe-guarding time-intervals. In the case of ground target suppression, a formation of UAVs must also break up and execute a coordinated maneuver to arrive at pre-defined positions over the target at the same time.

In both cases, only relative (rather than absolute) temporal constraints are given *a priori*, a critical point that needs to be emphasized. Furthermore, the vehicles must execute maneuvers in close proximity to each other. In addition, as pointed out in [1,2], the flow of information among vehicles may be severely restricted, either for security reasons or because of tight bandwidth limitations. As a consequence, no vehicle might be able to communicate with the entire formation and the amount of information that can be exchanged might be limited. Moreover, the topology of the inter-vehicle communications network supporting the cooperative mission may change over time. Under these circumstances, it is important to develop cooperative motion control strategies that can yield robust performance in the presence of time-varying communications networks arising from temporary loss of communications links and switching communications topologies.

Motivated by these and similar problems, there has been over the past few years increasing interest in the study of multi-agent system networks with applications to engineering and science problems. The range of topics addressed include parallel computing [3], synchronization of oscillators [4], study of collective behavior and flocking [5], multi-system consensus mechanisms [6], multi-vehicle system formations [7], coordinated motion control [8], asynchronous protocols [9], dynamic graphs [10], stochastic graphs [10–12], and graph-related theory [2, 13]. Especially relevant are the applications of the theory developed in the area of multi-vehicle formation control: spacecraft formation flying [14], UAV control [15, 16], coordinated control of land robots [8], and control of multiple autonomous underwater vehicles (AUVs) [17, 18]. In spite of significant progress in the field, much work remains to be done to develop strategies capable of yielding robust performance of a fleet of vehicles in the presence of complex vehicle dynamics, communications constraints, and partial vehicle failures.

It is against this backdrop of ideas that in this paper we address the problem of *steering a fleet of UAVs along desired paths while meeting stringent spatial and temporal constraints*. A representative example is the challenging mission scenario where a fleet of vehicles is tasked to cooperatively execute collision-free maneuvers and arrive at their final destinations at the same time (time-critical operations). In the adopted setup, the vehicles are assigned desired nominal paths and speed profiles along them. The paths are then appropriately parameterized, and the vehicles are requested to execute cooperative path following, rather than "open-loop" trajectory tracking maneuvers. This strategy yields robust performance in the face of external disturbances by allowing the vehicles to negotiate their speeds along the paths in response to information exchanged over the supporting communications network. The paper builds upon previous work by the authors on cooperative path following and extends it to a very general framework that allows for the consideration of *complex vehicle dynamics* and *time-varying communications topologies* in a rigorous mathematical setting. The reader is referred to [19–24] and the references therein for an introduction to the subject and a general perspective of the circle of ideas that are at the root of the present work. See also [25–31] and the textbook [32] for interesting and related pioneering work with applications to marine robots.

The core concepts and methods leading to the present paper can be tracked back to [23], where the authors addressed the problem of steering a group of vehicles along pre-defined spatial paths while holding a desired time-varying geometrical formation pattern. The solution proposed consists of two basic steps: first, a path-following control law is designed to drive each vehicle to its assigned path, with a nominal speed profile that may be path dependent. To this effect, each vehicle is made to approach a virtual target that moves along the path according to a conveniently defined dynamic law. In the second step, the speeds of the virtual targets (also called coordination states) are adjusted about their nominal values so as to synchronize their positions and achieve, indirectly, vehicle coordination. In the problem formulation, it was explicitly considered that each vehicle transmits its coordination state to a subset of the other vehicles only, as determined by the communications topology adopted. It was shown that the system that is obtained by putting together the path-following and coordination subsystems can be naturally viewed as either the feedback or the cascade connection of the latter two. Using this fact and recent results from nonlinear systems and graph theory, conditions were derived under which the path-following and coordination errors are driven to a neighborhood of zero in the presence of communication losses and time delays. Two different situations were considered. The first one captures the case where the communications graph is alternately

connected and disconnected (brief connectivity losses). The second reflects an operational scenario where the union of the communications graphs over uniform intervals of time remains connected (uniformly connected in mean). However, *no time-critical issues were addressed*.

The extension of the key concepts introduced in [23] to deal with time-critical issues can be found in [19,21, 22]. Especially relevant is the work reported in [19], where a general framework for the problem of cooperative control of multiple autonomous vehicles that must operate under strict spatial and temporal constraints was presented. The framework proposed borrows from multiple disciplines and integrates algorithms for path generation, path following, time-critical coordination, and $\mathcal{L}_1$ adaptive control theory for fast and robust adaptation. Together, these techniques yield control laws that meet strict performance requirements in the presence of modeling uncertainties and environmental disturbances.

The methodology proposed in [19], exemplified for the case of UAVs, unfolds in three basic steps. First, given a multiple vehicle task, a set of feasible trajectories is generated for all UAVs using an expedite method that takes explicitly into account the initial and the final boundary conditions, a general performance criterion to be optimized, the simplified UAV dynamics, and safety rules for collision avoidance. The second step consists of making each vehicle follow its assigned path while tracking a desired speed profile. Path-following control design is first done at a kinematic level, leading to an outer-loop controller that generates pitch- and yaw-rate commands to an inner-loop controller. The latter relies on off-the-shelf autopilots for angular-rate command tracking, augmented with an $\mathcal{L}_1$ adaptive output-feedback control law that guarantees stability and performance of the complete system for each vehicle in the presence of modeling uncertainties and environmental disturbances. Finally, in the third step, the speed profile of each vehicle is adjusted about the nominal speed profile derived in the first step to enforce the temporal constraints that must be met in real time in order to coordinate the entire fleet of UAVs. In this step, *it is assumed that the vehicles exchange information over a fixed communications network*. The results of path-following flight tests with a single vehicle are reported; see also [24]. However, despite the large number of simulations *no actual flight tests were done to assess the efficacy of the developed cooperative motion control strategy*.

The extension of the above introduced concepts to time-varying communications networks was first studied in [21]. Related work can also be found in [20], which proposes a new multiple vehicle control architecture aimed at reducing the frequency at which the information is exchanged among the vehicles by incorporating logic-based communications. To this effect, the authors borrow from and expand some of the key ideas exposed in [33, 34], where decentralized controllers for distributed systems were derived by using, for each system, its local state information together with estimates of the states of the systems that it communicates with. In [20], a key constraint was introduced: each system (vehicle) is only allowed to communicate with a set of immediate neighbors. With the scheme adopted, each vehicle decides when to transmit information to the neighbors by comparing its actual state with its estimate "as perceived" by the neighboring systems, and transmitting data when the "difference" between the two exceeds a certain level. As a consequence, the systems communicate at discrete instants of time, asynchronously.

The present paper borrows key ideas and design methods from previous work by the authors on cooperative path following and extends them to a very general setting that allows for the consideration of *complex vehicle dynamics*, *time-critical constraints*, and *time-varying communications topologies*. From a technical point of view, the paper departs substantially from previous published work in three key aspects:

(i) it puts forward a new algorithm for path following in 3-D space that overcomes the problems that arise from using local parameterizations of the rotation matrices;

(ii) it offers a new proof of convergence of the relevant variables involved in cooperative path following that significantly simplifies the one summarized in [21] and extends it to the case where the speed profiles of the different vehicles along their paths are arbitrary but meet desired geometrical constraints. In this setup, the communications graph that captures the underlying communications network topology is allowed to be disconnected during some interval of time or may even fail to be connected at all times. It is shown that if the connectivity of the communications graph satisfies a certain persistency of excitation (PE)-like condition, then the UAVs "reach consensus" in the sense that a conveniently defined cooperation error converges to a neighborhood of the origin; and

(iii) finally, flight test results of a coordinated road search mission that exploits the multi-UAV cooperative control framework developed in the paper demonstrate the efficacy of the developed algorithms.

This paper is organized as follows. Section II formulates the time-critical cooperative path-following problem, describes the kinematics of the systems of interest, and introduces a set of assumptions and limi-

tations on the supporting communications network. Section III presents a path-following control algorithm for UAVs in 3-D space. Section IV derives a strategy for time-critical cooperative path following of multiple UAVs in the presence of time-varying communications networks that relies on the adjustment of the desired speed profile of each vehicle. Section V addresses the stability and convergence properties of the combined coordination and path-following systems. Section VI presents actual flight test results performed in Camp Roberts, CA. Finally, Section VII summarizes the key results and contains the main conclusions.

Notation

Throughout the paper we use the following notation. $\{v\}_F$ is used to denote the vector v resolved in frame $\mathcal{F}$; $\{\vec{e}\}_F$ represents the versor $\vec{e}$ resolved in frame $\mathcal{F}$; $\omega_{F1/F2}$ denotes the angular velocity of frame $\mathcal{F}1$ with respect to frame $\mathcal{F}2$; the rotation matrix from frame $\mathcal{F}1$ to frame $\mathcal{F}2$ is represented by R_{F1}^{F2}; and $\dot{v}\,]_F$ indicates that the time-derivative of vector v is taken in frame $\mathcal{F}$. Moreover, unless otherwise noted, $\|\cdot\|$ is used for both the 2-norm of a vector and the induced 2-norm of a matrix.

II. Time-Critical Cooperative Path Following: Problem Formulation

This section provides a rigorous formulation of the problem of time-critical cooperative path-following control for multiple UAVs in 3-D space, in which a fleet of UAVs is tasked to converge to and follow a set of desired feasible paths so as to meet spatial and temporal constraints. We also introduce a set of assumptions and limitations on the supporting communications network.

We note that the problem of cooperative *path generation* is not addressed in this paper. In fact, we assume that a set of desired 3-D time trajectories $\Phi_{d,i}(t_d) : \mathbb{R} \to \mathbb{R}^3$, conveniently parameterized by a single time variable $t_d \in [0, t_d^*]$, are known for all the n UAVs involved in a cooperative mission. The variable t_d represents a *desired mission time* (distinct from the actual mission time that evolves as the mission unfolds), with t_d^* being the *desired mission duration*. For a given t_d, $\Phi_{d,i}(t_d)$ defines the desired position of the ith UAV t_d seconds after the initiation of the cooperative mission. From these time trajectories, *spatial paths* $p_{d,i}(\tau_{\ell,i}) : \mathbb{R} \to \mathbb{R}^3$ and the corresponding *desired speed profiles* $v_{d,i}(t_d) : \mathbb{R} \to \mathbb{R}$ can be easily derived for all the UAVs. For convenience, we parameterize each spatial path by its path length $\tau_{\ell,i} \in [0, \ell_{fi}]$, where ℓ_{fi} denotes the total length of the ith path, whereas the desired speed profiles are parameterized by the desired mission time t_d. It is assumed that both the paths and the speed profiles satisfy collision-avoidance constraints as well as appropriate boundary and feasibility conditions, such as those imposed by the physical limitations of the UAVs. It is further assumed that the rate and speed commands required to follow the paths and achieve time-coordination do not result in the UAVs operating outside their normal flight envelope and do not lead to internal saturation of the onboard autopilots. The problem of generation of feasible collision-free trajectories for multiple cooperative autonomous vehicles is described in detail in [35].

II.A. Path Following for a Single UAV

Pioneering work in the area of path following can be found in [36], where an elegant solution to the problem was presented for a wheeled robot at the kinematic level. In the setup adopted, the kinematic model of the vehicle was derived with respect to a Frenet-Serret frame moving along the path, while playing the role of a *virtual target vehicle* to be tracked by the real vehicle. The origin of the Frenet-Serret was placed at the point on the path closest to the real vehicle. This work spurred a great deal of activity in the literature addressing the path-following control problem. Of particular interest is the work reported in [37], in which the authors reformulated the setup used in [36] and derived a feedback control law that steers the dynamic model of a wheeled robot along a desired path and overcomes stringent initial condition constraints present in [36]. The key to the algorithm in [37] is to explicitly control the rate of progression of the virtual target along the path. This effectively creates an extra degree of freedom that can be exploited to avoid singularities that occur when the distance to the path is not well defined.

The solution to the path-following problem described in the present paper extends to the 3-D case the algorithm presented in [37], and relies on the insight that a UAV can follow a given path using only its attitude, thus leaving its speed as an extra degree of freedom to be used at the coordination level. The key idea of the algorithm is to use the vehicle's attitude control effectors to follow a virtual target vehicle running along the path. To this effect, following the approach adopted in [37], we introduce a frame attached

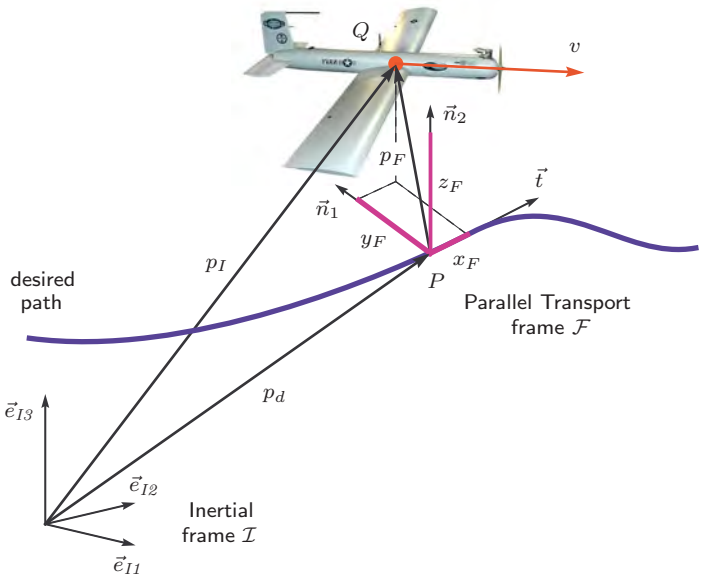

Figure 1. Following a virtual target vehicle. Problem geometry.

to this virtual target and define a generalized error vector between this moving coordinate system and a frame attached to the actual vehicle. With this setup, the path-following control problem is reduced to that of driving this generalized error vector to zero by using only the UAV's attitude control effectors, while following an arbitrary feasible speed profile. Next, we characterize the dynamics of the kinematic errors between the ith vehicle and its virtual target.

Figure 1 captures the geometry of the problem at hand. Let $p_d(\cdot)$ be the desired path assigned to one of the UAVs, and let ℓ_f be its total length. Let $\mathcal{I}$ denote an inertial reference frame $\{\vec{e}_{I1}, \vec{e}_{I2}, \vec{e}_{I3}\}$, and let $p_I(t)$ be the position of the center of mass Q of the UAV in this inertial frame. Further, let P be an arbitrary point on the desired path that plays the role of the virtual target, and let $p_d(\ell)$ denote its position in the inertial frame. Here $\ell \in [0, \ell_f]$ is a free length variable that defines the position of the virtual target vehicle along the path. In the setup adopted, the total rate of progression of the virtual target along the path is an extra design parameter. This approach is in striking contrast with the strategy used in the path-following algorithm introduced in [36], where P is defined as the point on the path that is closest to the vehicle. Endowing the point P with an extra degree of freedom is the key to the path-following algorithm presented in [37] and its extension to the 3-D case described in this paper.

For our purposes, it is convenient to define a *parallel transport frame* $\mathcal{F}$ attached to the point P on the path and characterized by the orthonormal vectors $\{\vec{t}(\ell), \vec{n}_1(\ell), \vec{n}_2(\ell)\}$, which satisfy the following frame equations [38,39]

$$\begin{bmatrix} \frac{\mathrm{d}\vec{t}}{\mathrm{d}\ell}(\ell) \\ \frac{\mathrm{d}\vec{n}_1}{\mathrm{d}\ell}(\ell) \\ \frac{\mathrm{d}\vec{n}_2}{\mathrm{d}\ell}(\ell) \end{bmatrix} = \begin{bmatrix} 0 & k_1(\ell) & k_2(\ell) \\ -k_1(\ell) & 0 & 0 \\ -k_2(\ell) & 0 & 0 \end{bmatrix} \begin{bmatrix} \vec{t}(\ell) \\ \vec{n}_1(\ell) \\ \vec{n}_2(\ell) \end{bmatrix},$$

where $k_1(\ell)$ and $k_2(\ell)$ are related to the polar coordinates of curvature $\kappa(\ell)$ and torsion $\tau(\ell)$ as

$$\kappa(\ell) = \left(k_1^2(\ell) + k_2^2(\ell)\right)^{\frac{1}{2}}, \qquad \tau(\ell) = -\frac{\mathrm{d}}{\mathrm{d}\ell}\left(\tan^{-1}\left(\frac{k_2(\ell)}{k_1(\ell)}\right)\right).$$

The vectors $\{\vec{t}, \vec{n}_1, \vec{n}_2\}$ define an orthonormal basis for $\mathcal{F}$, in which the unit vector $\vec{t}(\ell)$ defines the tangent direction to the path at the point determined by ℓ, while $\vec{n}_1(\ell)$ and $\vec{n}_2(\ell)$ define the normal plane perpendicular to $\vec{t}(\ell)$. We note that, unlike the Frenet-Serret frame, this moving frame is well defined when the path has a vanishing second derivative. This orthonormal basis can be used to construct the rotation matrix $R_F^I(\ell) = [\{\vec{t}(\ell)\}_I; \{\vec{n}_1(\ell)\}_I; \{\vec{n}_2(\ell)\}_I]$ from $\mathcal{F}$ to $\mathcal{I}$. Furthermore, the angular velocity of $\mathcal{F}$ with respect to $\mathcal{I}$,

resolved in $\mathcal{F}$, can be easily expressed in terms of the parameters $k_1(\ell)$ and $k_2(\ell)$ as

$$\{\omega_{F/I}\}_F = \left[\begin{array}{ccc} 0, & -k_2(\ell)\,\dot{\ell}, & k_1(\ell)\,\dot{\ell} \end{array}\right]^\top .$$

Let $p_F(t)$ be the position of the vehicle's center of mass Q in the parallel transport frame, and let $x_F(t)$, $y_F(t)$, and $z_F(t)$ be the components of the vector $p_F(t)$ with respect to the basis $\{\vec{t}, \vec{n}_1, \vec{n}_2\}$, that is,

$$\{p_F\}_F = \left[\begin{array}{ccc} x_F, & y_F, & z_F \end{array}\right]^\top .$$

Finally, let $\mathcal{W}$ denote a vehicle-carried *velocity frame* $\{\vec{w}_1, \vec{w}_2, \vec{w}_3\}$ with its origin at the UAV center of mass and its x-axis aligned with the velocity vector of the UAV. The z-axis is chosen to lie in the plane of symmetry of the UAV, and the y-axis is determined by completing the right-hand system. In this paper, $q(t)$ and $r(t)$ are the y-axis and z-axis components, respectively, of the vehicle's rotational velocity resolved in the $\mathcal{W}$ frame. With a slight abuse of notation, $q(t)$ and $r(t)$ will be referred to as *pitch rate* and *yaw rate*, respectively, in the $\mathcal{W}$ frame.

With the above notation, we next characterize the kinematic error dynamics of the UAV with respect to the virtual target. We start by deriving the *position*-error dynamics. For this purpose, we note that

$$p_I = p_d(\ell) \; + \; p_F \,,$$

from which it follows that

$$\dot{p}_I]_I = \dot{\ell}\,\vec{t} \; + \; \omega_{F/I} \times p_F \; + \; \dot{p}_F]_F,$$

where $\cdot]_I$ and $\cdot]_F$ are used to indicate that the derivatives are taken in the inertial and parallel transport frames, respectively. Because

$$\dot{p}_I]_I = v\,\vec{w}_1 \,,$$

where $v(t)$ denotes the magnitude of the UAV's ground velocity vector, the path-following kinematic *position*-error dynamics of the UAV with respect to the virtual target can be written as

$$\dot{p}_F]_F = -\,\dot{\ell}\,\vec{t} \; - \; \omega_{F/I} \times p_F \; + \; v\,\vec{w}_1 \,. \tag{1}$$

To derive the *attitude*-error dynamics of the UAV with respect to its virtual target, we first introduce an auxiliary frame $\mathcal{D}$ $\{\vec{b}_{1D}, \vec{b}_{2D}, \vec{b}_{3D}\}$, which will be used to shape the approach attitude to the path as a function of the "cross-track" error components y_F and z_F. The frame $\mathcal{D}$ has its origin at the UAV center of mass and the vectors $\vec{b}_{1D}(t)$, $\vec{b}_{2D}(t)$, and $\vec{b}_{3D}(t)$ are defined as

$$\vec{b}_{1D} \triangleq \frac{d\,\vec{t} - y_F\,\vec{n}_1 - z_F\,\vec{n}_2}{(d^2 + y_F^2 + z_F^2)^{\frac{1}{2}}} \,, \qquad \vec{b}_{2D} \triangleq \frac{y_F\,\vec{t} + d\,\vec{n}_1}{(d^2 + y_F^2)^{\frac{1}{2}}} \,, \qquad \vec{b}_{3D} \triangleq \vec{b}_{1D} \times \vec{b}_{2D} \,, \tag{2}$$

with d being a (positive) constant characterizing distance. The basis vector $\vec{b}_{1D}(t)$ defines the desired direction of the UAV's velocity vector. Clearly, when the vehicle is far from the desired path, the vector $\vec{b}_{1D}(t)$ becomes perpendicular to $\vec{t}(\ell)$. As the vehicle comes closer to the path and the cross-track error becomes smaller, then $\vec{b}_{1D}(t)$ tends to $\vec{t}(\ell)$. The rotation matrix $R_D^F(t) \in \mathsf{SO(3)}$ is given by

$$R_D^F = \left[\begin{array}{ccc} \frac{d}{(d^2+y_F^2+z_F^2)^{\frac{1}{2}}} & \frac{y_F}{(d^2+y_F^2)^{\frac{1}{2}}} & \frac{z_F d}{(d^2+y_F^2+z_F^2)^{\frac{1}{2}}(d^2+y_F^2)^{\frac{1}{2}}} \\ \frac{-y_F}{(d^2+y_F^2+z_F^2)^{\frac{1}{2}}} & \frac{d}{(d^2+y_F^2)^{\frac{1}{2}}} & \frac{-y_F z_F}{(d^2+y_F^2+z_F^2)^{\frac{1}{2}}(d^2+y_F^2)^{\frac{1}{2}}} \\ \frac{-z_F}{(d^2+y_F^2+z_F^2)^{\frac{1}{2}}} & 0 & \frac{(d^2+y_F^2)^{\frac{1}{2}}}{(d^2+y_F^2+z_F^2)^{\frac{1}{2}}} \end{array}\right] .$$

Next, let $\tilde{R}(t) \in \mathsf{SO(3)}$ be the rotation matrix from $\mathcal{W}$ to $\mathcal{D}$, that is,

$$\tilde{R} \triangleq R_W^D = R_F^D\,R_W^F = (R_D^F)^\top\,R_W^F \,,$$

and define the real-valued error function on $\mathsf{SO(3)}$

$$\Psi(\tilde{R}) \triangleq \frac{1}{2}\mathrm{tr}\left[\left(\mathbb{I}_3 - \Pi_R^\top \Pi_R\right)\left(\mathbb{I}_3 - \tilde{R}\right)\right] , \tag{3}$$

where Π_R is defined as

$$\Pi_R \triangleq \begin{bmatrix} 0 & 1 & 0 \\ 0 & 0 & 1 \end{bmatrix}.$$

The function $\Psi(\tilde{R})$ in (3) can be expressed in terms of the entries of $\tilde{R}(t)$ as

$$\Psi(\tilde{R}) = \frac{1}{2}\left(1 - \tilde{R}_{11}\right),$$

where $\tilde{R}_{11}(t)$ denotes the $(1,1)$ entry of $\tilde{R}(t)$. Therefore, $\Psi(\tilde{R})$ is positive-definite about $\tilde{R}_{11} = 1$. We note that $\tilde{R}_{11} = 1$ corresponds to the situation where the velocity vector of the UAV is aligned with the basis vector $\vec{b}_{1D}(t)$, which defines the desired attitude.

The attitude kinematics equation

$$\dot{\tilde{R}} = \dot{R}_W^D = R_W^D \left(\{\omega_{W/D}\}_W\right)^\wedge = \tilde{R}\left(\{\omega_{W/D}\}_W\right)^\wedge,$$

where $(\cdot)^\wedge : \mathbb{R}^3 \to \mathsf{SO}(3)$ denotes the *hat map* (see Appendix A), can be used to derive the time derivative of $\Psi(\tilde{R})$, given by

$$\dot{\Psi}(\tilde{R}) = -\frac{1}{2}\mathrm{tr}\left[\left(\mathbb{I}_3 - \Pi_R^\top \Pi_R\right)\tilde{R}\left(\{\omega_{W/D}\}_W\right)^\wedge\right].$$

Property (45) of the hat map (see Appendix A) leads to

$$\dot{\Psi}(\tilde{R}) = \frac{1}{2}\left(\left(\left(\mathbb{I}_3 - \Pi_R^\top \Pi_R\right)\tilde{R} - \tilde{R}^\top\left(\mathbb{I}_3 - \Pi_R^\top \Pi_R\right)\right)^\vee\right)^\top \{\omega_{W/D}\}_W,$$

where $(\cdot)^\vee : \mathsf{SO}(3) \to \mathbb{R}^3$ denotes the *vee map*, which is defined as the inverse of the hat map. Moreover, since the first component of $\left(\left(\mathbb{I}_3 - \Pi_R^\top \Pi_R\right)\tilde{R} - \tilde{R}^\top\left(\mathbb{I}_3 - \Pi_R^\top \Pi_R\right)\right)^\vee$ is equal to zero, we can also write

$$\begin{aligned}\dot{\Psi}(\tilde{R}) &= \frac{1}{2}\left(\left(\left(\mathbb{I}_3 - \Pi_R^\top \Pi_R\right)\tilde{R} - \tilde{R}^\top\left(\mathbb{I}_3 - \Pi_R^\top \Pi_R\right)\right)^\vee\right)^\top \Pi_R^\top \Pi_R \{\omega_{W/D}\}_W \\ &= \left(\frac{1}{2}\Pi_R\left(\left(\mathbb{I}_3 - \Pi_R^\top \Pi_R\right)\tilde{R} - \tilde{R}^\top\left(\mathbb{I}_3 - \Pi_R^\top \Pi_R\right)\right)^\vee\right)^\top \Pi_R \{\omega_{W/D}\}_W. \end{aligned} \tag{4}$$

Next, we define the attitude error $e_{\tilde{R}}(t)$ as

$$e_{\tilde{R}} \triangleq \frac{1}{2}\Pi_R\left(\left(\mathbb{I}_3 - \Pi_R^\top \Pi_R\right)\tilde{R} - \tilde{R}^\top\left(\mathbb{I}_3 - \Pi_R^\top \Pi_R\right)\right)^\vee,$$

which allows to rewrite (4) in the more compact form

$$\dot{\Psi}(\tilde{R}) = e_{\tilde{R}} \cdot \left(\Pi_R \{\omega_{W/D}\}_W\right).$$

We note that the attitude error $e_{\tilde{R}}(t)$ can also be expressed in terms of the entries of $\tilde{R}(t)$ as

$$e_{\tilde{R}} = \frac{1}{2}\begin{bmatrix} \tilde{R}_{13}, & -\tilde{R}_{12} \end{bmatrix}^\top,$$

and therefore, within the region where $\Psi(\tilde{R}) < 1$, we have that if $\|e_{\tilde{R}}\| = 0$, then $\tilde{R}_{11} = 1$. Finally, noting that $\{\omega_{W/F}\}_W$ can be expressed as

$$\{\omega_{W/D}\}_W = \{\omega_{W/I}\}_W - \tilde{R}^\top\left(R_F^D\{\omega_{F/I}\}_F + \{\omega_{D/F}\}_D\right),$$

we obtain

$$\dot{\Psi}(\tilde{R}) = e_{\tilde{R}} \cdot \left(\begin{bmatrix} q \\ r \end{bmatrix} - \Pi_R \tilde{R}^\top\left(R_F^D\{\omega_{F/I}\}_F + \{\omega_{D/F}\}_D\right)\right). \tag{5}$$

This equation describes the path-following kinematic *attitude*-error dynamics of the frame $\mathcal{W}$ with respect to the frame $\mathcal{D}$. The path-following kinematic-error dynamics $\mathcal{G}_e$ can now be obtained by combining (1) and (5), yielding

$$\begin{aligned} \dot{p}_F]_F &= -\,\dot{\ell}\,\vec{t} \;-\; \omega_{F/I} \times p_F \;+\; v\,\vec{w}_1\,, \\ \dot{\Psi}(\tilde{R}) &= e_{\tilde{R}} \cdot \left(\begin{bmatrix} q \\ r \end{bmatrix} - \Pi_R \tilde{R}^\top \left(R_F^D \{\omega_{F/I}\}_F + \{\omega_{D/F}\}_D \right) \right) . \end{aligned} \tag{6}$$

In the kinematic-error model (6), $q(t)$ and $r(t)$ play the role of control inputs, while the rate of progression $\dot{\ell}(t)$ of the point P along the path becomes an extra variable that can be manipulated at will. At this point, we formally define the path-following generalized error vector $x_{pf}(t)$ as

$$x_{pf} \triangleq \begin{bmatrix} p_F^\top, & e_{\tilde{R}}^\top \end{bmatrix}^\top .$$

Notice that, within the region where $\Psi(\tilde{R}) < 1$, if $x_{pf} = 0$, then both the path-following position error and the path-following attitude error are equal to zero, that is, $p_F = 0$ and $\tilde{R}_{11} = 0$.

Using the above formulation, and given a spatially defined feasible path $p_d(\cdot)$, we now define the problem of *path following* for a single vehicle.

Definition 1 (Path-Following Problem (PFP)) *For a given UAV, design feedback control laws for pitch rate $q(t)$, yaw rate $r(t)$, and rate of progression $\dot{\ell}(t)$ of the virtual target along the path such that all closed-loop signals are bounded and the path-following generalized error vector $x_{pf}(t)$ converges to a neighborhood of the origin, regardless of what the temporal speed assignment of the mission is (as long as it is physically feasible).*

Stated in simple terms, the problem above amounts to designing feedback laws so that a UAV converges to and remains inside a tube centered on the desired path curve assigned to this UAV, for an arbitrary speed profile (subject to feasibility constraints).

II.B. Time-Critical Coordination and Network Model

To enforce the temporal constraints that must be met in real time to coordinate the entire fleet of vehicles, the speed profile of each vehicle is adjusted based on coordination information exchanged among the UAVs over a time-varying communications network. To this effect, an appropriate coordination variable needs to be defined for each vehicle that captures the objective of the cooperative mission, in our case, simultaneous arrival of all the UAVs at their final destinations.

For this purpose, we start by defining $\ell'_{d,i}(t_d)$ as the desired normalized curvilinear abscissa of the ith UAV along its corresponding path at the desired mission time t_d, which is given by

$$\ell'_{d,i}(t_d) \triangleq \frac{1}{\ell_{fi}} \int_0^{t_d} v_{d,i}(\sigma_t)\, d\sigma_t\,, \tag{7}$$

with ℓ_{fi} and $v_{d,i}(\cdot)$ being, respectively, the length of the path and the desired speed profile corresponding to the ith UAV. The trajectory-generation algorithm ensures that the desired speed profiles $v_{d,i}(\cdot)$ satisfy feasibility conditions, which implies that the following bounds hold for all vehicles:

$$0 < v_{\min} \le v_{d,i\,\min} \le v_{d,i}(\cdot) \le v_{d,i\,\max} \le v_{\max}\,, \qquad\qquad i = 1, \ldots, n\,, \tag{8}$$

where $v_{\min}$ and $v_{\max}$ denote, respectively, the minimum and maximum operating speeds of the UAV, while $v_{d,i\,\min}$ and $v_{d,i\,\max}$ denote lower and upper bounds on the desired speed profile for the ith UAV. From the definition of $\ell'_{d,i}(t_d)$ and the bounds in (8), it follows that $\ell'_{d,i}(t_d)$ is a strictly increasing continuous function of t_d mapping $[0, t_d^*]$ into $[0, 1]$, and satisfying $\ell'_{d,i}(0) = 0$ and $\ell'_{d,i}(t_d^*) = 1$. We also define $\eta_i : [0, 1] \to [0, t_d^*]$ to be the inverse function of $\ell'_{d,i}(t_d)$, $t_d \in [0, t_d^*]$. Clearly, $\eta_i(\cdot)$ is also a strictly increasing continuous function

of its argument. Then, letting $\ell'_i(t)$ be the normalized curvilinear abscissa at time t of the ith virtual target vehicle running along its path, defined as

$$\ell'_i(t) \triangleq \frac{\ell_i(t)}{\ell_{fi}},$$

where $\ell_i(t) \in [0, \ell_{fi}]$ was introduced in the previous section, we define the time-dependent variables

$$\xi_i(t) \triangleq \eta_i(\ell'_i(t)), \qquad i = 1, \ldots, n. \tag{9}$$

From this definition, it follows that $\xi(t) \in [0, t^*_d]$, and therefore this variable can be seen as a *virtual time* that characterizes the status of the mission for the ith UAV at time t in terms of the desired mission time t_d.

We note that, for any two vehicles i and j, if $\xi_i(t) = \xi_j(t) = t'_d$ at a given time t, then $\ell'_i(t) = \ell'_{d,i}(t'_d)$ and $\ell'_j(t) = \ell'_{d,j}(t'_d)$, which implies that at time t the target vehicles corresponding to UAVs i and j have the desired relative position along the path at the desired mission time t'_d. Clearly, if $\xi_i(t) = \xi_j(t)$ for all $t \geq 0$, then the ith and jth virtual target vehicles maintain desired relative position along the path at all times and, in particular, these two target vehicles arrive at their final destinations at the same time, which does not necessarily correspond to the desired mission duration t^*_d. Also, in the case of collision avoidance in time (see [35]), if $\xi_i(t) = \xi_j(t)$ for all $t \geq 0$, then the solution to the path-generation problem ensures that the virtual targets i and j do not collide. Moreover, if the ith virtual target travels at the desired speed for all time in the interval $[0, t]$, that is, $\dot{\ell}_i(\tau) = v_{d,i}(\tau)$ for all $\tau \in [0, t]$, then we have that $\ell_i(\tau) = \ell_{d,i}(\tau)$ for all $\tau \in [0, t]$, which implies that $\xi_i(\tau) = \tau$ (or equivalently, that $\dot{\xi}_i(\tau) = 1$) for all $\tau \in [0, t]$. This set of properties makes the variables $\xi_i(t)$ an appropriate metric for vehicle coordination, and therefore we will refer to them as *coordination states*. We notice that the use of these specific coordination variables is motivated by the work in [22].

To meet the desired temporal assignments of the cooperative mission, these coordination states are to be exchanged among the UAVs over the supporting communications network. Next, we use tools and facts from *algebraic graph theory* to model the information exchange over the time-varying network as well as the constraints imposed by the communications topology. The reader is referred to [40] for key concepts and details on algebraic graph theory.

First, in order to account for the communications constraints imposed by this inter-vehicle network, we assume that the ith UAV can only exchange information with a neighboring set of vehicles, denoted here by G_i. We also assume that the communications between two UAVs is bidirectional and that the information is transmitted continuously with no delays. Moreover, since the flow of information among vehicles may be severely restricted, either for security reasons or because of tight bandwidth limitations, we impose the constraint that each vehicle only exchanges its coordination state $\xi_i(t)$ with its neighbors. Finally, we assume that the connectivity of the communications graph $\Gamma(t)$ that captures the underlying bidirectional communications network topology of the fleet at time t satisfies the persistency of excitation (PE)-like condition

$$\frac{1}{n}\frac{1}{T}\int_t^{t+T} Q\, L(\tau)\, Q^\top d\tau \geq \mu\, \mathbb{I}_{n-1}, \qquad \text{for all } t \geq 0, \tag{10}$$

where $L(t) \in \mathbb{R}^{n\times n}$ is the Laplacian of the graph $\Gamma(t)$, and Q is an $(n-1)\times n$ matrix such that $Q1_n = 0$ and $QQ^\top = \mathbb{I}_{n-1}$, with 1_n being the vector in $\mathbb{R}^n$ whose components are all 1. The parameters $T, \mu > 0$ characterize the quality of service (QoS) of the communications network, which in the context of this paper represents a measure of the level of connectivity of the communications graph. We note that the PE-like condition (10) requires only the communications graph $\Gamma(t)$ to be connected in an integral sense, not pointwise in time. In fact, the graph may be disconnected during some interval of time or may even fail to be connected for the entire duration of the mission. Similar type of conditions can be found, for example, in [41] and [6].

Using the formulation above, we next define the problem of *time-critical cooperative path following* for a fleet of n UAVs.

Definition 2 (Time-Critical Cooperative Path-Following Problem (TC-CPFP)) *Given a fleet of n vehicles supported by an inter-vehicle communications network and a set of desired 3-D time trajectories $\Phi_{d,i}(t_d)$, design feedback control laws for pitch rate $q(t)$, yaw rate $r(t)$, and speed $v(t)$ such that*

1. *all closed-loop signals are bounded;*

2. *for each vehicle i, $i \in \{1,\dots,n\}$, the path-following generalized error vector $x_{pf,i}(t)$ converges to a neighborhood of the origin; and*

3. *for each pair of vehicles i and j, $i,j \in \{1\dots,n\}$, the coordination error $|\xi_i(t)-\xi_j(t)|$ converges to a neighborhood of the origin, guaranteeing (quasi-)simultaneous time of arrival and ensuring collision-free maneuvers.*

At this point, we stress that in this paper we address the design of control algorithms for path following and time coordination yielding robust performance of a fleet of UAVs executing various time-critical cooperative missions. These control algorithms are to be seen as guidance *outer-loop* controllers that provide reference commands to *inner-loop* autopilots stabilizing the UAV dynamics and providing angular-rate as well as speed tracking capabilities. This inner-outer loop approach simplifies the design process and affords the designer a systematic approach to seamlessly tailor the algorithms for a very general class of UAVs that come equipped with inner-loop commercial autopilots. In the next section, we present a set of assumptions on the inner closed-loop performance of the UAVs with their autopilots, which will be useful to analyze the convergence properties of the path-following and coordination control laws developed later in the paper.

II.C. Unmanned Aerial Vehicle with Autopilot

As mentioned in the previous section, this paper addresses the design of outer-loop control laws for path following and time-critical cooperation of a fleet of small tactical UAVs. The design of inner-loop onboard autopilots that are capable of tracking reference commands generated by outer-loop controllers and providing uniform performance across the flight envelope is beyond the scope of the work presented here. Nevertheless, it is important to determine performance requirements for the onboard autopilot that ensure that the mission is successfully accomplished by the fleet of vehicles. To this effect, and for the purpose of this paper, we will assume that each UAV is equipped with an onboard autopilot designed to stabilize the UAV and to provide angular-rate as well as speed tracking capabilities. In particular, we make the assumption that the onboard autopilots ensure that each UAV is able to track bounded pitch-rate and yaw-rate commands, denoted here by $q_c(t)$ and $r_c(t)$, with guaranteed performance bounds γ_q and γ_r. Stated mathematically,

$$|q_c(t)-q(t)| \le \gamma_q\,, \qquad \forall\ t \ge 0\,, \tag{11a}$$

$$|r_c(t)-r(t)| \le \gamma_r\,, \qquad \forall\ t \ge 0\,. \tag{11b}$$

Similarly, we assume that, if the speed commands $v_c(t)$ satisfy the bounds

$$v_{\min} \le v_c(\tau) \le v_{\max}\,, \qquad \forall\ \tau \in [0,t]\,, \tag{12}$$

then the autopilots ensure that each UAV tracks its corresponding speed command with guaranteed performance bound γ_v:

$$|v_c(\tau)-v(\tau)| \le \gamma_v\,, \qquad \forall\ \tau \in [0,t]\,. \tag{13}$$

The bounds γ_q, γ_r, and γ_v characterize thus the level of tracking performance that the inner-loop autopilot is able to provide. These bounds will be used later in the paper to derive design constraints for the inner-loop tracking performance that guarantee stability of the complete cooperative control architecture.

It is also important to note that, in this setup, it is the autopilot that determines the bank angle required to track the angular-rate commands $q_c(t)$ and $r_c(t)$. Therefore, it is justified to assume that the UAV roll dynamics (roll rate and bank angle) are bounded for bounded angular-rate commands corresponding to the set of feasible paths considered.

For the missions of interest, typical off-the-shelf autopilots are capable of providing uniform performance across the flight envelope of small UAVs while operating in nominal conditions. However, these commercial autopilots may fail to provide adequate performance across the operational envelope in the event of actuator failures, vehicle damage, or in the presence of adverse environmental disturbances. Under these unfavorable circumstances, adaptive augmentation loops are seen as an appealing technology that can improve vehicle performance. In [24, 42], for example, we present an $\mathcal{L}_1$ adaptive control architecture for autopilot augmentation that retains the properties of the onboard commercial autopilot, and adjusts the autopilot commands only when the tracking performance degrades. Figure 2 shows the inner-loop control architecture considered in [24, 42], with the adaptive augmentation loop wrapped around the autopilot. The adaptive controller

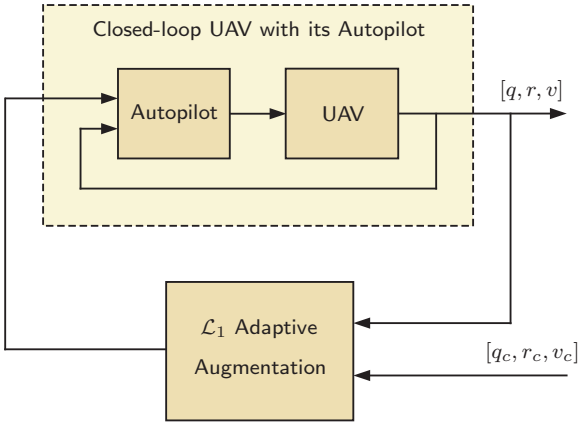

Figure 2. Inner-loop control structure with the $\mathcal{L}_1$ adaptive augmentation loop [24, 42].

uses angular-rate and speed measurements to modify the commands generated by the outer-loop algorithms, which are then sent to the autopilot as references to be tracked. This structure for autopilot augmentation does not require any modifications to the autopilot itself, and at the same time it does not use internal states of the autopilot for control design purposes.

III. 3-D Path Following for a Single UAV

This section describes an outer-loop 3-D path-following nonlinear control algorithm that uses vehicle angular rates to steer the ith vehicle along the spatial path $p_{d,i}(\cdot)$ for an arbitrary feasible speed profile (temporal assignment along the path). Controller design builds on previous work by the authors on path-following control of small tactical UAVs, reported in [24], and derives new path-following control laws on $\mathsf{SO(3)}$ that avoid the geometric singularities and complexities that appear when dealing with local parameterizations of the vehicle's attitude. First, we address only the kinematic equations of the UAV by taking pitch rate and yaw rate as virtual outer-loop control inputs. In particular, we show that there exist stabilizing functions for $q(t)$ and $r(t)$ leading to local exponential stability of the origin of $\mathcal{G}_e$ with a prescribed domain of attraction. Then, we perform a stability analysis for the case of non-perfect inner-loop tracking and show that the path-following errors are locally uniformly ultimately bounded with the same domain of attraction. The results yield an efficient methodology to design path-following controllers for UAVs with due account for the vehicle kinematics and the characteristics of their inner-loop autopilots.

III.A. Nonlinear Control Design using UAV Kinematics

Recall from Section II.A that the main objective of the path-following control algorithm is to drive the position error $p_F(t)$ and the attitude error $e_{\tilde{R}}(t)$ to zero. At the kinematic level, these objectives can be achieved by determining feedback control laws for $q(t)$, $r(t)$, and $\dot{\ell}(t)$ that ensure that the origin of the kinematic-error equations in (6) is exponentially stable with a given domain of attraction. Figure 3 presents the kinematic closed-loop system considered in this section.

To solve the path-following problem, we first let the rate of progression of point P along the path be governed by

$$\dot{\ell} = (v\,\vec{w}_1 + K_\ell p_F)\cdot\vec{t}, \tag{14}$$

where K_ℓ is a positive constant gain. Then, the rate commands $q_c(t)$ and $r_c(t)$ given by

$$\begin{bmatrix} q_c \\ r_c \end{bmatrix} \triangleq \Pi_R \tilde{R}^\top \left(R_F^D\{\omega_{F/I}\}_F + \{\omega_{D/F}\}_D\right) - 2K_{\tilde{R}} e_{\tilde{R}}, \tag{15}$$

where $K_{\tilde{R}}$ is also a positive constant gain, drive the path-following generalized error vector $x_{pf}(t)$ to zero with a guaranteed rate of convergence. A formal statement of this result is given in the lemma below.

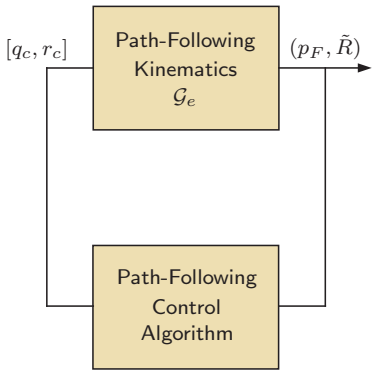

Figure 3. Path-following closed-loop system for a single UAV solved at a kinematic level.

Lemma 1 *Assume that the UAV speed $v(t)$ verifies the following bounds:*

$$0 < v_{\min} \leq v(t) \leq v_{\max}\,, \qquad \forall\, t \geq 0\,. \tag{16}$$

If, for given positive constants $c < \frac{1}{\sqrt{2}}$ and c_1, we choose the path-following control parameters K_ℓ, $K_{\tilde{R}}$, and d such that

$$K_{\tilde{R}}\, K_p > \frac{v_{\max}^2}{c_1^2(1-2c^2)^2}\,, \tag{17}$$

where K_p is defined as

$$K_p \triangleq \min\left\{K_\ell,\, \frac{v_{\min}}{(d^2 + c^2 c_1^2)^{\frac{1}{2}}}\right\}, \tag{18}$$

then the rate commands in (15), together with the law in (14) for the rate of progression of the virtual target along the path, ensure that the origin of the kinematic-error equations in (6) is exponentially stable with guaranteed rate of convergence

$$\lambda_{pf}^* \triangleq \frac{K_p + K_{\tilde{R}}(1-c^2)}{2} - \frac{1}{2}\left(\left(K_p - K_{\tilde{R}}(1-c^2)\right)^2 + \frac{4(1-c^2)}{c_1^2(1-2c^2)^2}\, v_{\max}^2\right)^{\frac{1}{2}} \tag{19}$$

and domain of attraction

$$\Omega_c \triangleq \left\{(p_F, \tilde{R}) \in \mathbb{R}^3 \times \mathsf{SO(3)} \;\middle|\; \Psi(\tilde{R}) + \frac{1}{c_1^2}\|p_F\|^2 \leq c^2 < \frac{1}{2}\right\}. \tag{20}$$

Proof: The proof of this result, which uses some insight from [43], is given in Appendix B.

Remark 1 *The choice of the characterizing distance d in the definition of the auxiliary frame $\mathcal{D}$ (see (2)) can be used to adjust the rate of convergence for the path-following closed-loop system. This is consistent with the fact that a large parameter d reduces the penalty for cross-track position errors, which results in a slow rate of convergence of the UAV to the path. Insights into this path-following control algorithm can be found in [44].*

III.B. Stability Analysis for Non-Perfect Inner-Loop Tracking

The stabilizing control laws in (14) and (15) lead to local exponential stability of the origin of the path-following kinematic-error dynamics (6) with a prescribed domain of attraction. In general, this result does not hold when the dynamics of the UAV are included in the problem formulation. In this section, we perform a stability analysis of the path-following closed-loop system for the case of non-ideal inner-loop tracking. In particular, we assume that the onboard autopilot ensures that the UAV is able to track bounded pitch-rate and yaw-rate commands with the performance bounds in (11) and show that the path-following errors $p_F(t)$ and $e_{\tilde{R}}(t)$ are locally uniformly ultimately bounded with the same domain of attraction Ω_c. The next lemma states this result formally.

Lemma 2 *Assume that the UAV speed $v(t)$ verifies the bounds in (16). For given positive constants $c < \frac{1}{\sqrt{2}}$ and c_1, choose the path-following control parameters K_ℓ, $K_{\tilde{R}}$, and d according to the design constraint in (17). Further, let δ_{pf} be a positive constant verifying*

$$0 < \delta_\lambda < \lambda^*_{pf}\,, \tag{21}$$

where λ^*_{pf} was defined in (19). If the performance bounds γ_q and γ_r in (11) satisfy the following inequality:

$$\gamma_\omega \triangleq \left(\gamma_q^2 + \gamma_r^2\right)^{\frac{1}{2}} < \frac{2\,c}{(1-c^2)^{\frac{1}{2}}}\,\delta_\lambda\,, \tag{22}$$

then, for any initial state $(p_F(0), \tilde{R}(0)) \in \Omega_c$, the rate commands in (15), together with the law in (14) for the rate of progression of the virtual target along the path, ensure that there is a time $T_b \geq 0$ such that the path-following errors $p_F(t)$ and $e_{\tilde{R}}(t)$ satisfy

$$\|e_{\tilde{R}}(t)\|^2 + \frac{1}{c_1^2}\|p_F(t)\|^2 \leq \left(\frac{1}{1-c^2}\|e_{\tilde{R}}(0)\| + \frac{1}{c_1^2}\|p_F(0)\|\right) \mathrm{e}^{-2(\lambda^*_{pf}-\delta_\lambda)t}\,, \qquad \forall\ 0 \leq t < T_b\,, \tag{23}$$

$$\|e_{\tilde{R}}(t)\|^2 + \frac{1}{c_1^2}\|p_F(t)\|^2 \leq \frac{(1-c^2)\,\gamma_\omega^2}{4\delta_\lambda^2}\,, \qquad \forall\ t \geq T_b\,. \tag{24}$$

Proof: The proof of this result is given in Appendix C.

Remark 2 *Inequalities (23) and (24) show that the path-following errors $p_F(t)$ and $e_{\tilde{R}}(t)$ are uniformly bounded for all $t \geq 0$ and uniformly ultimately bounded with ultimate bounds*

$$\|e_{\tilde{R}}(t)\| \leq \frac{(1-c^2)^{\frac{1}{2}}}{2\delta_\lambda}\,\gamma_\omega\,, \qquad \forall\ t \geq T_b\,,$$

$$\|p_F(t)\| \leq \frac{c_1(1-c^2)^{\frac{1}{2}}}{2\delta_\lambda}\,\gamma_\omega\,, \qquad \forall\ t \geq T_b\,.$$

These ultimate bounds are proportional to the inner-loop tracking performance bound γ_ω and, in the limit ideal case of perfect inner-loop tracking, one recovers the exponential stability result derived in Lemma 1.

IV. Time-Critical Coordination

The previous section offered a solution to the path-following problem for a single vehicle and an arbitrary feasible speed profile by using a control strategy in which the vehicle's attitude control effectors are used to follow a virtual target running along the path. We now address the problem of time-critical cooperative control of multiple vehicles. To this effect, the speeds of the vehicles are adjusted based on coordination information exchanged among the vehicles over a time-varying network. In particular, the outer-loop coordination control law is intended to provide a correction to the desired speed profile $v_{d,i}(\cdot)$ obtained in the trajectory-generation step, and to generate a total speed command $v_{c,i}(t)$. This speed command is then to be tracked by the ith vehicle to achieve coordination in time.

We start by recalling from Section II.B that the main objective of the time-critical cooperative algorithm is to drive the coordination errors $|\xi_i(t) - \xi_j(t)|$ to a neighborhood of the origin. To solve this coordination problem, we first note that the evolution of the ith coordination state is given by

$$\dot{\xi}_i(t) = \frac{\mathrm{d}}{\mathrm{d}t}\Big(\eta_i\left(\ell_i'(t)\right)\Big) = \left.\frac{\mathrm{d}\eta_i}{\mathrm{d}\ell_i'}\right|_{\ell_i'(t)} \dot{\ell}_i'(t)\,.$$

From the definitions of $\ell'_{d,i}(\cdot)$ and $\eta_i(\cdot)$, we have that the following equality holds for all $\ell_i' \in [0,1]$:

$$\ell'_{d,i}\left(\eta_i(\ell_i')\right) = \ell_i'\,,$$

from which one can show that

$$\left.\frac{\mathrm{d}\eta_i}{\mathrm{d}\ell_i'}\right|_{\ell_i'} = \frac{1}{\frac{1}{\ell_{fi}} v_{d,i}(\eta_i(\ell_i'))}\,, \qquad \forall\ \ell_i' \in [0,1]\,.$$

Then, the time derivative of the ith coordination state can be expressed as

$$\dot{\xi}_i(t) = \frac{\dot{\ell}_i(t)}{v_{d,i}(\xi_i(t))}\,.$$

Next, we recall from the solution to the path-following problem that the evolution of the ith virtual target vehicle along the path is given by

$$\dot{\ell}_i = (v_i\,\vec{w}_{1,i} + K_\ell\,p_{F,i})\cdot\vec{t}_i\,,$$

where for simplicity we keep K_ℓ without indexing and we drop the dependency of the various variables on t. The dynamics of the ith coordination state can thus be rewritten as

$$\dot{\xi}_i = \frac{(v_i\,\vec{w}_{1,i} + K_\ell\,p_{F,i})\cdot\vec{t}_i}{v_{d,i}(\xi_i)}\,.$$

At this point, it is important to remark that, if the path-following control law can guarantee that, for every UAV, the quantity $(\vec{w}_{1,i}\cdot\vec{t}_i)$ is positive and bounded away form zero for all $t \geq 0$, that is,

$$\vec{w}_{1,i}\cdot\vec{t}_i \geq c_2 > 0\,, \qquad \forall\; t \geq 0\,, \quad \forall\; i \in \{1,\ldots,n\}\,, \tag{25}$$

where $0 < c_2 \leq 1$, then, to solve the coordination problem, we can use dynamic inversion and define the speed command for the ith vehicle as

$$v_{c,i} \triangleq \frac{u_{\text{coord},i}\,v_{d,i}(\xi_i) - K_\ell\,p_{F,i}\cdot\vec{t}_i}{\vec{w}_{1,i}\cdot\vec{t}_i}\,, \tag{26}$$

where $u_{\text{coord},i}(t)$ is a coordination control law, yet to be defined. With this speed command, the partially closed-loop coordination dynamics for the ith target vehicle can be rewritten as

$$\dot{\xi}_i = u_{\text{coord},i} + \frac{e_{v,i}}{v_{d,i}(\xi_i)}\,\vec{w}_{1,i}\cdot\vec{t}_i\,, \tag{27}$$

where $e_{v,i}(t) \triangleq v_i(t) - v_{c,i}(t)$ denotes the velocity tracking error for the ith vehicle. In what follows, we assume that the bound in (25) holds for every vehicle and derive a coordination control law $u_{\text{coord},i}(t)$ that achieves coordination for the entire fleet of UAVs. This assumption will be verified later in Section V, where we derive an expression for the constant c_2, and prove stability of the combined time-critical cooperative path-following closed-loop system.

Recall now that each vehicle is allowed to exchange only its coordination parameter $\xi_i(t)$ with its neighbors G_i, which are defined by the possibly time-varying communications topology. To observe this constraint, we propose the decentralized coordination law

$$u_{\text{coord},1}(t) = -a\sum_{j\in G_1}(\xi_1(t) - \xi_j(t)) + 1\,, \tag{28a}$$

$$u_{\text{coord},i}(t) = -a\sum_{j\in G_i}(\xi_i(t) - \xi_j(t)) + \chi_{I,i}(t)\,, \qquad i = 2,\ldots,n\,, \tag{28b}$$

$$\dot{\chi}_{I,i}(t) = -b\sum_{j\in G_i}(\xi_i(t) - \xi_j(t))\,, \qquad \chi_{I,i}(0) = 1\,, \qquad i = 2,\ldots,n\,, \tag{28c}$$

where vehicle 1 is elected as the formation leader (which can be a *virtual vehicle*), and a and b are positive adjustable coordination control gains. Note that the coordination control law has a proportional-integral structure, which provides disturbance rejection capabilities at the coordination level. Moreover, we note that the vehicles exchange information only about the corresponding virtual targets, rather than exchanging their own state information. The importance of this observation can hardly be overemphasized. The benefits of using "virtual information" in consensus problems are illustrated in [45].

The coordination law in (28) can be rewritten in compact form as

$$\begin{aligned} u_{\text{coord}}(t) &= -aL(t)\,\xi(t) + \left[\begin{smallmatrix}1\\ \chi_I(t)\end{smallmatrix}\right]\,,\\ \dot{\chi}_I(t) &= -b\,C^\top L(t)\,\xi(t)\,, \qquad \chi_{I,i}\,(0) = 1\,, \end{aligned} \tag{29}$$

where $\xi(t) \triangleq [\xi_1(t), \ldots, \xi_n(t)]^\top$, $u_{\text{coord}}(t) \triangleq [u_{\text{coord},1}(t), \ldots, u_{\text{coord},n}(t)]^\top$, $\chi_I(t) \triangleq [\chi_{I,2}(t), \ldots, \chi_{I,n}(t)]^\top$, $C^\top \triangleq [\ 0 \quad \mathbb{I}_{n-1}\ ]$, and $L(t)$ is the Laplacian of the undirected graph $\Gamma(t)$ that captures the underlying bidirectional communications network topology of the UAV formation at time t. It is well known that the Laplacian of an undirected graph is symmetric, $L^\top(t) = L(t)$, and positive semi-definite, $L(t) \geq 0$; $\lambda_1(L(t)) = 0$ is an eigenvalue with eigenvector 1_n, $L(t)1_n = 0$; and the second smallest eigenvalue of $L(t)$ is positive if and only if the graph $\Gamma(t)$ is connected, that is,

$$\min_{\substack{x \neq 0 \\ 1_n^\top x = 0}} \frac{x^\top L(t) x}{\|x\|^2} \;=\; \lambda_2(L(t)) \;>\; 0 \qquad \Leftrightarrow \qquad \Gamma(t) \text{ connected}\,.$$

Next, we reformulate the coordination problem stated above into a stabilization problem. To this end, we define the *projection matrix* Π as

$$\Pi \triangleq \mathbb{I}_n - \frac{1_n 1_n^\top}{n}\,,$$

and we note that $\Pi = \Pi^\top = \Pi^2$ and also that $Q^\top Q = \Pi$, where Q is the $(n-1) \times n$ matrix introduced in (10). Moreover, we have that $L(t)\,\Pi = \Pi\,L(t) = L(t)$, and the spectrum of the matrix $\bar{L}(t) \triangleq Q\,L(t)\,Q^\top$ is equal to the spectrum of $L(t)$ without the eigenvalue $\lambda_1 = 0$ corresponding to the eigenvector 1_n. Finally, we define the coordination error state $\zeta(t) \triangleq [\zeta_1(t)^\top, \zeta_2(t)^\top]^\top$ as

$$\begin{aligned} \zeta_1(t) &\triangleq Q\,\xi(t) \\ \zeta_2(t) &\triangleq \chi_I(t) - 1_{n-1}\,. \end{aligned}$$

By definition, $\zeta_1(t) = 0$ is equivalent to $\xi(t) \in \text{span}\{1_n\}$, which implies that, if $\zeta(t) = 0$, then all target vehicles are coordinated at time t.

With the above notation, the closed-loop coordination dynamics formed by (27) and the coordination control algorithm defined in (29) can be reformulated as

$$\dot{\zeta}(t) = F(t)\,\zeta(t) \;+\; H\,e'_v(t)\,, \tag{30}$$

where $F(t) \in \mathbb{R}^{(2n-2)\times(2n-2)}$ and $H \in \mathbb{R}^{(2n-2)\times n}$ are given by

$$F(t) \triangleq \begin{bmatrix} -a\bar{L}(t) & QC \\ -bC^\top Q^\top \bar{L}(t) & 0 \end{bmatrix}\,, \qquad H \triangleq \begin{bmatrix} Q \\ 0 \end{bmatrix}\,,$$

and $e'_v(t) \in \mathbb{R}^n$ is a vector with its ith component being equal to $e'_{v,i} \triangleq \frac{e_{v,i}}{v_{d,i}(\xi_i)}\,\vec{w}_{1,i} \cdot \vec{t}_i$.

Next we show that, if the connectivity of the communications graph $\Gamma(t)$ verifies the PE-like condition (10) and, in addition, every vehicle travels at the commanded speed $v_{c,i}(t)$ (that is, $e_{v,i}(t) \equiv 0$), then the coordinated system asymptotically reaches agreement and all the vehicles travel at the desired speed

$$\begin{aligned} \lim_{t\to\infty} (\xi_i(t) - \xi_j(t)) = 0\,, \qquad & \forall\, i, j \in \{1, \ldots, n\} \\ \lim_{t\to\infty} \dot{\xi}(t) = 1_n\,. & \end{aligned}$$

On the other hand, if $e_{v,i}(t) \neq 0$ for some $t \geq 0$, then the coordination error vector degrades gracefully with the *size* of speed tracking error $e_v(t) \triangleq [e_{v,1}(t), \ldots, e_{v,n}(t)]^\top$. The next lemma summarizes this result.

Lemma 3 *Consider the coordination system (30) and suppose that the Laplacian of the graph that models the communications topology satisfies the PE-like condition (10) for some parameters μ and T. Moreover, assume that the speed tracking error vector $e_v(t)$ is bounded for all $t \geq 0$. Then, there exist coordination control gains a and b such that the system (30) is input-to-state stable (ISS) with respect to $e_v(t)$, satisfying*

$$\|\zeta(t)\| \leq k_1 \|\zeta(0)\| \mathrm{e}^{-\lambda_c t} + k_2 \sup_{\tau \in [0,t)} \|e_v(\tau)\|\,, \qquad \forall\, t \geq 0\,, \tag{31}$$

for some (computable) positive constants k_1 and k_2, and with

$$\lambda_c \geq \bar{\lambda}_c \triangleq \frac{an\mu}{(1+anT)^2}\,\frac{1}{2n\sqrt{n}+1}\,.$$

Furthermore, the coordination states $\xi_i(t)$ and their rates of variation $\dot{\xi}_i(t)$ satisfy

$$\lim_{t\to\infty} \sup |\xi_i(t) - \xi_j(t)| \leq k_3 \lim_{t\to\infty} \sup \|e_v(t)\|, \tag{32}$$

$$\lim_{t\to\infty} \sup |\dot{\xi}_i(t) - 1| \leq k_4 \lim_{t\to\infty} \sup \|e_v(t)\|\,, \tag{33}$$

for all $i, j \in \{1, \ldots, n\}$, and for some (computable) positive constants k_3 and k_4.

Proof: The proof of this result is given in Appendix D.

Remark 3 *Lemma 3 above indicates that the QoS of the network (characterized by the parameters T and μ) limits the achievable (guaranteed) rate of convergence for the coordination control loop. According to the lemma, for a given QoS of the network, the maximum (guaranteed) rate of convergence $\bar{\lambda}_c^*$ is achieved by setting $a^* = \frac{1}{Tn}$, which results in*

$$\bar{\lambda}_c^* = \frac{\mu}{4T} \frac{1}{2n\sqrt{n}+1}\,.$$

Also, it is important to mention that, as the parameter T goes to zero (graph connected pointwise in time), the convergence rate can be set arbitrarily fast by increasing the coordination control gains a and b. This is consistent with results obtained in previous work by the authors (see [46, Lemma 2]).

Finally, we notice that

$$\bar{\gamma}_\lambda \triangleq \frac{an\mu}{(1+anT)^2}$$

represents the (guaranteed) convergence rate for the coordination loop with a proportional control law, rather than a proportional-integral control law (see Appendix D). It is straightforward to verify that, for a given proportional gain a, we have that $\bar{\lambda}_c < \bar{\gamma}_\lambda$, which implies that a proportional control law can provide higher rates of convergence than the proportional-integral control law used in this paper. However, as mentioned earlier, the integral term in the coordination control law is important in the current application as it provides disturbance rejection capabilities at the coordination level.

V. Combined Path Following and Time-Critical Cooperation

In the previous sections we have shown that, under an appropriate set of assumptions, the path-following and coordination control laws are able to ensure stability and ultimate boundedness of the path-following and time-critical cooperation problems when treated separately. In particular, the solution developed for the path-following problem assumes that the speed of the UAV is bounded above and below, while the control law designed for vehicle coordination relies on the assumption that the angle between the UAV's velocity vector and the tangent direction to the path is less than 90 deg (see assumptions (16) and (25)). This section addresses the convergence properties of the combined cooperation and path-following systems, and derives design constraints for the inner-loop tracking performance bounds that guarantee stability of the complete system. The cooperative path-following control architecture for the ith UAV is presented in Figure 4.

In this section, we assume that the onboard autopilot ensures that each UAV is able to track bounded pitch-rate, yaw-rate, as well as speed commands with the performance bounds in (11)-(13). At this point, we note that, while the pitch-rate and yaw-rate commands in (15) are continuous in time, the same cannot be said about the speed command in (26). In fact, due to the time-varying nature of the network topology, the coordination law $u_{\text{coord}}(t)$ in (28) is discontinuous, which implies that the speed command $v_c(t)$ is also discontinuous. Assuming that the following bound holds for all vehicles and for all $t \geq 0$,

$$|v_{c,i}(t) - v_i(t)| \leq \gamma_v\,, \qquad i = 1, \ldots, n\,, \tag{34}$$

which implies that

$$\sup_{t\geq 0} \|e_v(t)\| \leq \sqrt{n}\,\gamma_v\,,$$

then the maximum amplitude $\Delta v_{c,i}$ of a jump in the speed command $v_{c,i}(t)$ can be derived from (26), (28) and the results of Lemma 3, and is given by

$$\Delta v_{c,i} \triangleq \frac{2a(n-1)v_{d,i\max}\left(k_1\|\zeta(0)\| + k_2\sqrt{n}\,\gamma_v\right)}{c_2}\,, \qquad i = 1, \ldots, n\,,$$

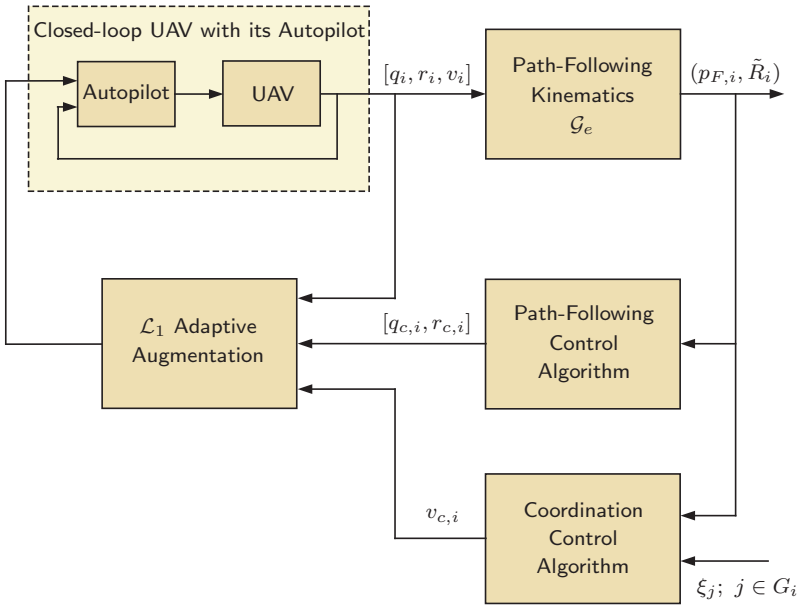

Figure 4. Time-critical cooperative path-following closed-loop for the ith vehicle with $\mathcal{L}_1$ augmentation.

where $v_{d,i\,\max}$ was introduced in (8). Thus, a necessary (but by no means sufficient) condition for the bound in (34) to hold is that

$$\Delta v_{c,i} < \gamma_v\,, \qquad\qquad i = 1, \ldots, n\,.$$

The above condition limits the choice of the coordination control gains, which in particular need to satisfy the following inequality

$$2a(n-1)v_{d,i\,\max}k_2\sqrt{n} < c_2\,, \qquad\qquad i = 1, \ldots, n\,.$$

However, the derivation of sufficient conditions that guarantee that the bound in (13) holds for all time requires assumptions on vehicle dynamics and autopilot design, and is thus beyond the scope of this paper. Hence, for the subsequent developments, we make the assumption that the bound in (13) holds –provided the speed command $v_{c,i}(t)$ satisfies the bounds in (12)–, and derive design constraints for this inner-loop tracking performance bound that ensure that the overall time-critical cooperative path-following control system is stable and has desired convergence properties. The next theorem summarizes this result.

Theorem 1 *Consider a fleet of n UAVs supported by a communications network that satisfies the PE-like condition in (10). Let c and c_1 be positive constants, with $c < \frac{1}{\sqrt{2}}$. For each UAV, choose the path-following control parameters K_ℓ, $K_{\tilde{R}}$, and d such that*

$$d > \frac{2c(1-c^2)^{\frac{1}{2}}}{1-2c^2}\,c_1\,, \tag{35}$$

$$K_{\tilde{R}}\,K_p > \frac{v_{\max}^2}{c_1^2(1-2c^2)^2}\,, \tag{36}$$

where K_p is defined as in (18). Also, choose the coordination control gains a and b such that

$$a > 0\,, \qquad\qquad b = \frac{2n}{2n\sqrt{n}+1}\,\frac{a^2 n\mu}{(1+anT)^2}\,, \tag{37}$$

and let k_1 and k_2 be the constants in (31) for this particular choice of control gains a and b. Further, let the

performance bounds γ_q, γ_r, *and* γ_v *satisfy the following inequalities:*

$$(\gamma_q^2+\gamma_r^2)^{\frac{1}{2}} < \frac{2c}{(1-c^2)^{\frac{1}{2}}}\,\delta_\lambda\,, \tag{38}$$

$$\gamma_v < \min\left\{\frac{v_{\max}c_2 - v_{d\max} - K_\ell cc_1}{c_2+\bar{k}_2 v_{d\max}\sqrt{n}}\,,\ \frac{v_{d\min}-v_{\min}-K_\ell cc_1}{1+\bar{k}_2 v_{d\max}\sqrt{n}}\right\}\,, \tag{39}$$

where δ_λ *is a constant satisfying* (21), $v_{d\max} \triangleq \max_{i=1,\ldots,n} v_{d,i\max}$, $v_{d\min} \triangleq \min_{i=1,\ldots,n} v_{d,i\min}$, *while* c_2 *and* $\bar{k}_2$ *are defined as:*

$$c_2 \triangleq \frac{d(1-2c^2)-2c_1c^2(1-c^2)^{\frac{1}{2}}}{(d^2+c^2c_1^2)^{\frac{1}{2}}}\,, \qquad \bar{k}_2 \triangleq (2a(n-1)+1)k_2\,.$$

Then, the progression law in (14), *the rate commands in* (15), *and the speed commands in* (26) *with the coordination control law in* (28) *ensure that, for all initial conditions*

$$(p_{F,i}(0), \tilde{R}_i(0)) \in \Omega_c\,, \qquad i=1,\ldots,n\,, \tag{40}$$

$$\|\zeta(0)\| \le \frac{1}{\bar{k}_1}\left(\min\left\{\frac{v_{\max}-\gamma_v}{v_{d\max}}c_2-1\,,\ \frac{v_{d\min}}{v_{d\max}}-\frac{v_{\min}+\gamma_v}{v_{d\max}}\right\}-\bar{k}_2\sqrt{n}\,\gamma_v-\frac{K_\ell cc_1}{v_{d\max}}\right)\,, \tag{41}$$

where $\bar{k}_1 \triangleq (2a(n-1)+1)k_1$, *there exist times* $T_{b,i} \ge 0$ *and a positive constant* $\lambda_c \le \bar{\lambda}_c$ *such that the path-following errors* $p_{F,i}(t)$ *and* $e_{\tilde{R},i}(t)$ *for the* i*th UAV satisfy*

$$\|e_{\tilde{R},i}(t)\|^2+\frac{1}{c_1^2}\|p_{F,i}(t)\|^2 \le \left(\frac{1}{1-c^2}\|e_{\tilde{R},i}(0)\|+\frac{1}{c_1^2}\|p_{F,i}(0)\|\right)\mathrm{e}^{-2(\lambda_{pf}^*-\delta_\lambda)t}\,, \qquad \forall\ 0\le t<T_{b,i}\,, \tag{42}$$

$$\|e_{\tilde{R},i}(t)\|^2+\frac{1}{c_1^2}\|p_{F,i}(t)\|^2 \le \frac{(1-c^2)\,\gamma_\omega^2}{4\delta_\lambda^2}\,, \qquad \forall\ t\ge T_{b,i}\,, \tag{43}$$

while the coordination error states $\zeta(t)$ *satisfy*

$$\|\zeta(t)\| \le k_1\|\zeta(0)\|\mathrm{e}^{-\lambda_c t}+k_2\sqrt{n}\,\gamma_v\,, \qquad \forall t\ge 0\,. \tag{44}$$

Proof: The proof of this result is given in Appendix E.

Remark 4 *Inequalities* (42) *and* (43) *show that the path-following errors* $p_{F,i}(t)$ *and* $e_{\tilde{R},i}(t)$ *are uniformly bounded for all* $t\ge 0$ *and uniformly ultimately bounded with ultimate bounds*

$$\|e_{\tilde{R},i}(t)\| \le \frac{(1-c^2)^{\frac{1}{2}}}{2\delta_\lambda}\,\gamma_\omega\,, \qquad \forall\ t\ge T_b\,, \quad \forall\ i\in\{1,\ldots,n\}\,,$$

$$\|p_{F,i}(t)\| \le \frac{c_1(1-c^2)^{\frac{1}{2}}}{2\delta_\lambda}\,\gamma_\omega\,, \qquad \forall\ t\ge T_b\,, \quad \forall\ i\in\{1,\ldots,n\}\,,$$

which are proportional to the inner-loop tracking performance bound γ_ω. *On the other hand, inequality* (44) *implies that the coordination error state* $\zeta(t)$ *converges exponentially fast to a neighborhood of the origin with radius proportional to the inner-loop speed tracking performance bound* γ_v. *This implies that, in the limit case of perfect inner-loop tracking, the path-following errors of each vehicle and the coordination error state vector converge exponentially fast to zero.*

VI. Cooperative Road Search with Multiple Unmanned Aerial Vehicles

In this section we discuss flight test results for a cooperative road-search mission that show the efficacy of the multi-vehicle cooperative control framework presented in this paper. Cooperative path-following missions involving multiple UAVs were flown for the first time at Camp Roberts, CA, in November 2009, and then demonstrated four more times at the same location in February, May, July, and November of 2010. More flight tests are expected in November 2011. The results in this section verify the main theoretical claims of the cooperative control algorithm presented in this paper and demonstrate the feasibility of the onboard implementation of the algorithms and the validity of the approach.

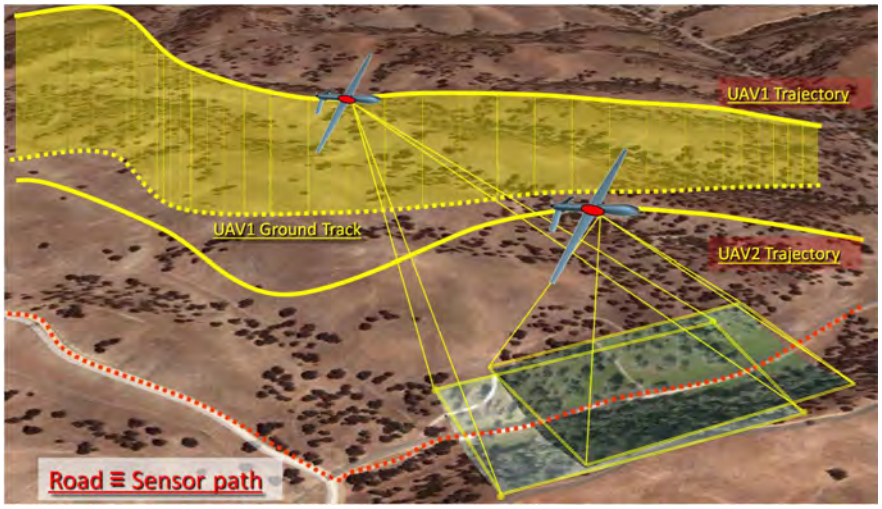

Figure 5. Coordinated road search using multiple UAVs.

VI.A. Mission description

One of the applications that motivates the use of multiple cooperative UAVs and poses several challenges to systems engineers, both from a theoretical and practical standpoint, is automatic road search for improvised explosive device detection; see Figure 5. The mission is initiated by a minimally trained user who scribbles a path on a digital map, generating a precise continuous ground-track for the airborne sensors to follow. This ground-track is then transmitted over the network to a fleet of small tactical UAVs equipped with complementary visual sensors. Decentralized optimization algorithms autonomously generate feasible flight trajectories that maximize road coverage and account for sensor capabilities –field of view, resolution, and gimbal constraints– as well as inter-vehicle and ground-to-air communications limitations. The fleet of UAVs then starts the cooperative road search. During this phase, the information obtained from the sensors mounted onboard the UAVs is shared over the network and retrieved by remote users in near real time. The explosive device detection can thus be done remotely on the ground, based on in-situ imagery data delivered over the network.

In this particular mission scenario, a robust cooperative control algorithm for the fleet of UAVs can improve mission performance and provide reliable target discrimination, by effectively combining the capabilities of the onboard sensors. In fact, flying in a coordinated fashion is what allows, for example, to maximize the overlap of the fields of view (FOVs) of multiple sensors and to take full advantage of complementary sensors.

VI.B. Airborne system architecture

The small tactical UAVs employed in this particular mission are two SIG Rascals 110 operated by NPS; see Figure 6. The two UAVs have the same avionics and the same instrumentation onboard, the only difference being the vision sensors. The first UAV has a bank-compensated high-resolution 12-MPx imagery camera, while the second UAV has a full-motion video camera suspended on a pan-tilt gimbal. Due to payload constraints, each UAV is allowed to carry only one camera at a time, and therefore the two cameras need to be mounted on different platforms. The rest of the onboard avionics, common to both platforms, includes two PC-104 industrial embedded computers [47] assembled in a stack, a wireless Mobile Ad-hoc Network (MANET) link [48], and the Piccolo Plus autopilot [49] with its dedicated 900-MHz command and control channel. Details of the complete airborne network-centric architecture are presented in Figure 7.

The first PC-104 computer acts as a secondary autopilot controller, running the cooperative-control algorithms in hard real time at 100 Hz and directly communicating with the Piccolo Plus autopilot at 50 Hz over a dedicated serial link. This connection efficiently eliminates communication delays between the outer-loop control algorithms and the autopilot. The second PC-104 is a mission management computer that implements a set of non-real-time routines enabling onboard preprocessing and retrieval of the sensory data –high-resolution imagery or video– in near real time over the network. Integration of the MANET link allows for robust transparent inter-vehicle and ground communication, which is needed for both the

(a) SIG Rascal 110 research aircraft.

(b) High-resolution camera.

(c) Full-motion video camera.

Figure 6. SIG Rascal UAV with two different onboard cameras.

coordination algorithms and the expedited sensory data delivery to a remote mission operator. In fact, the MANET link provides "any-to-any" connectivity capability, allowing every node –vehicle or ground station– to communicate directly with every other node. Moreover, information about the connectivity of the entire network can be retrieved in near real time. Details on the flight test architecture and the supporting network infrastructure for coordination control and data dissemination can be found in [48, 50].

VI.C. Flight Test Results

We now present flight test results for a cooperative road-search mission executed by the two SIG Rascals. The objective of the mission is to detect a target moving along a given road and, if detection occurs, to collect information about the target. This information is then to be shared over a MANET link so that it can be retrieved by remote mission operators in near real time. Success of the mission relies on the ability to overlap the footprint of the FOVs of the two cameras along the road, which increases the probability of target detection [51]. Next, we provide details about the execution of this coordinated road-search mission, which we divide in four consecutive phases, namely, initialization, transition, road search, and vision-based target tracking. The description is supported by one of the flight tests results performed during a Tactical Network Testbed field experiment at Camp Roberts, CA; see figures 8-11.

In the *initialization phase*, an operator specifies on a digital map the road of interest. Then, a centralized optimization algorithm generates road-search suboptimal paths and desired speed profiles for the two UAVs that explicitly account for UAV dynamic constraints, collision-avoidance constraints, and mission-specific constraints such as inter-vehicle and vehicle-to-ground communications limitations as well as sensory capabilities. In particular, the trajectory-generation algorithm is designed to maximize the overlap of the footprints of the FOVs of the high-resolution camera and the full-motion video during the road search. In addition to the road-search paths and the corresponding desired speed profiles, the outcome of the trajectory-generation algorithm includes a *sensor trajectory* on the ground to be followed by the vision sensors. The two road-search paths and the sensor path, along with the three corresponding speed profiles, are then transmitted to the UAVs over the MANET link.

In the *transition phase*, the two UAVs fly from their standby starting positions to the initial points of the respective road-search paths. For this purpose, decentralized optimization algorithms generate feasible

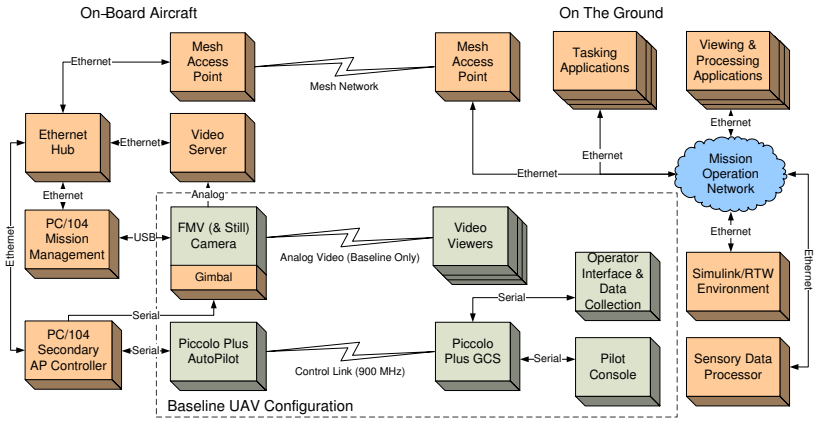

Figure 7. Network-Centric architecture of the airborne platform.

collision-free 3D trajectories to ensure that the two UAVs arrive at the initial points of the road-search paths at the same time. Once these transition trajectories are generated, the two vehicles start operating in cooperative path-following mode. From that moment on, the UAVs follow the transition paths while adjusting their speeds based on coordination information exchanged over the MANET link in order to achieve simultaneous arrival at the starting point of the road-search paths. The transition and road-search spatially-deconflicted paths obtained for this particular mission scenario, together with the corresponding desired speed profiles and the path separations, are shown in Figure 8. Figure 9 illustrates the performance of the coordination control algorithm during the transition phase of the mission.

The third phase addresses the *cooperative road-search mission* itself, in which the two UAVs follow the road-search paths generated in the initialization phase while adjusting their speeds to ensure the required overlap of the FOV footprints of the cameras. In this phase, a target vehicle running along the sensor path is virtually implemented on one of the UAVs. For this road-search mission, a natural choice for this sensor path is the road itself, and this virtual vehicle determines thus the spot of the road being observed by the vision sensors mounted onboard the UAVs at a given time. This virtual vehicle is indeed used as a leader in the coordination algorithm, and its speed is also adjusted, based on the coordination states of the two UAVs. The coordination state of this virtual vehicle is also transmitted over the tactical network and used in the coordination control laws of the two "real" vehicles. The performance of the cooperative path-following control algorithm is illustrated in Figure 10. For this particular mission scenario, the coordination errors remain below 7% during the entire duration of the road search, while the path-following cross-track errors converge to a 3 m tube around the desired spatial paths.

Finally, when a target is detected on the road, the two UAVs immediately switch to *cooperative vision-based tracking* mode. In this phase, the UAVs track the target by means of guidance loops that use visual information for feedback [52], while simultaneously providing in-situ imagery for precise geo-location of the point of interest. During this target-tracking phase, a coordination algorithm ensures that the two UAVs keep a predefined phase separation of $\frac{\pi}{2}$ rad while orbiting around the target. This coordination algorithm uses the decentralized coordination control law described in Section IV to adjust the orbiting speed of the UAVs, with the main difference that *phase on orbit* is now used as a coordination state, rather than virtual time. Besides collision avoidance, cooperation through phase-on-orbit coordination allows for several additional benefits, including reduced sensitivity to target escape maneuvers [53] and possible extraction of 3D information from 2D images [54]. The performance of the cooperative path-following control algorithm is illustrated in Figure 11, which shows the trajectories of the two UAVs while tracking the target as well as the phase-coordination error between the UAVs.

In summary, the results presented above demonstrate feasibility and efficiency of the onboard integration of the nonlinear path-following and coordination algorithms. During the flight experiments, the required control commands never exceeded the limits defined for the UAV in traditional waypoint navigation mode. At the same time, the achieved functionality of the UAV following 3D curves in an inertial space outperforms the conventional waypoint navigation method typically implemented on off-the-shelf commercial autopilots. These results provide also a roadmap for further development and onboard implementation of advanced cooperative algorithms, opening new frontiers for UAV operations.

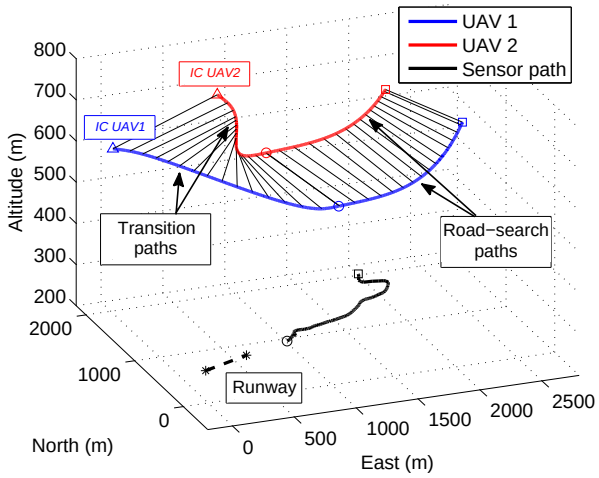

(a) Desired 3D spatial paths.

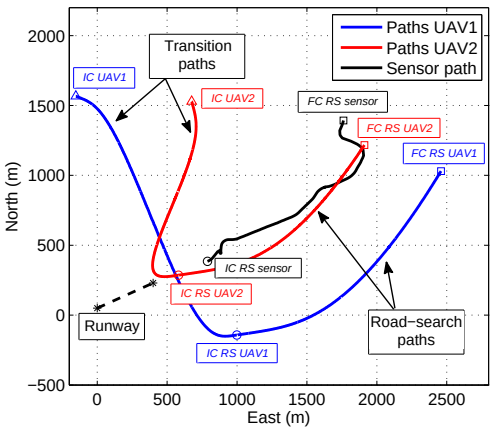

(b) 2D projections.

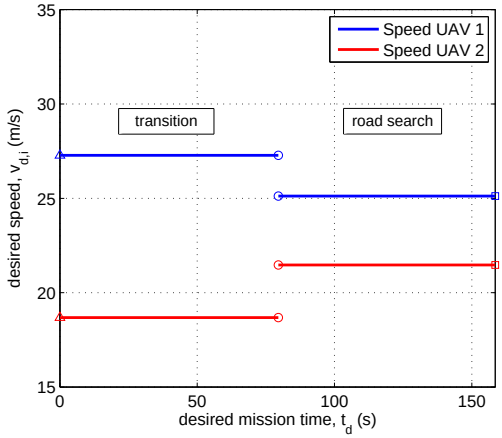

(c) Desired speed profiles.

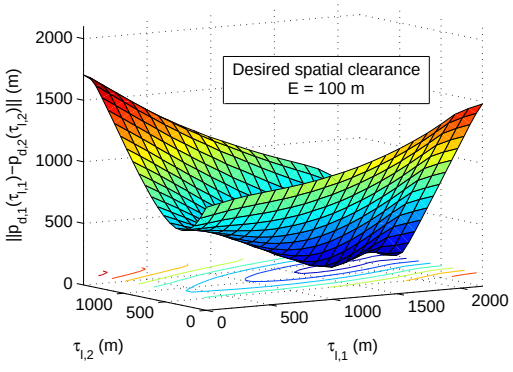

(d) Path separation for transition phase.

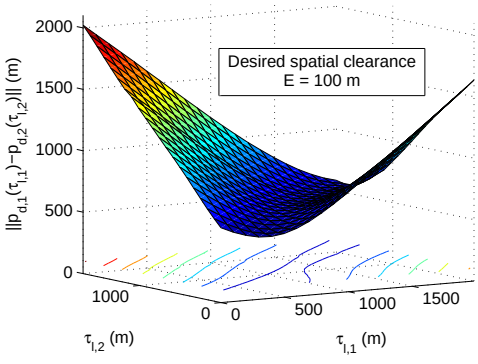

(e) Path separation for road-search phase.

Figure 8. Coordinated road-search trajectory generation.

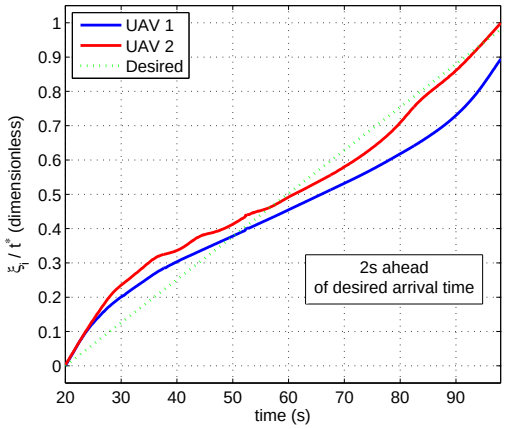

(a) Normalized coordination states.

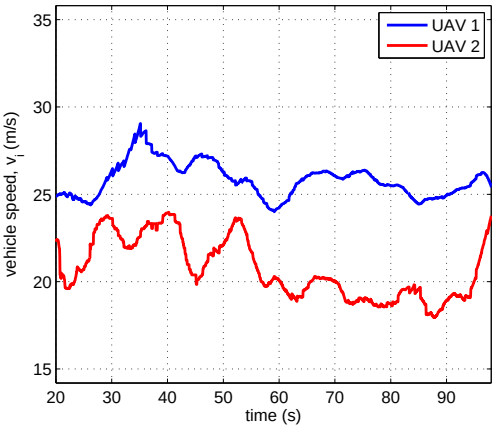

(b) UAV speeds.

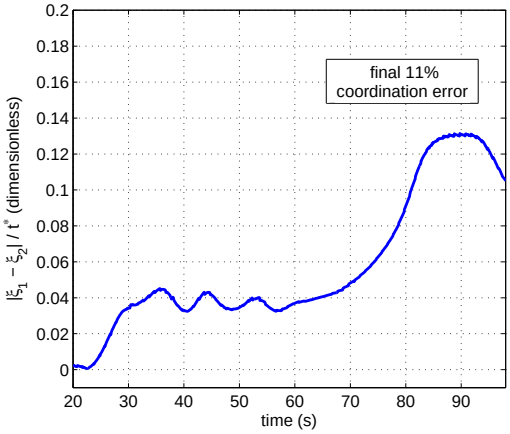

(c) Normalized coordination error.

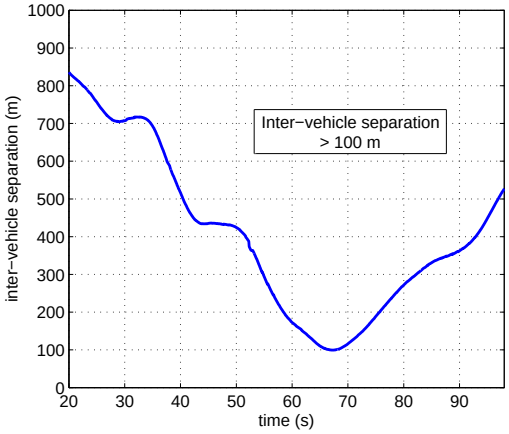

(d) Inter-vehicle separation.

Figure 9. Time-coordination during the transition phase.

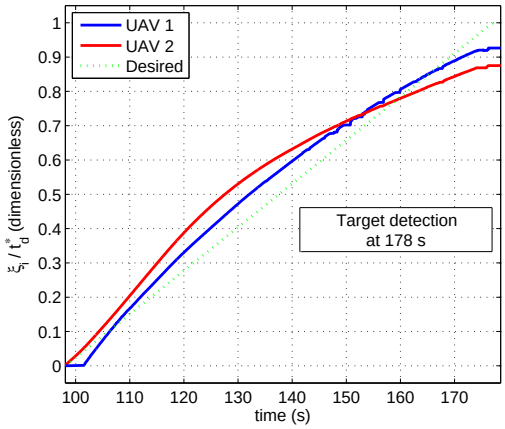

(a) Normalized coordination states.

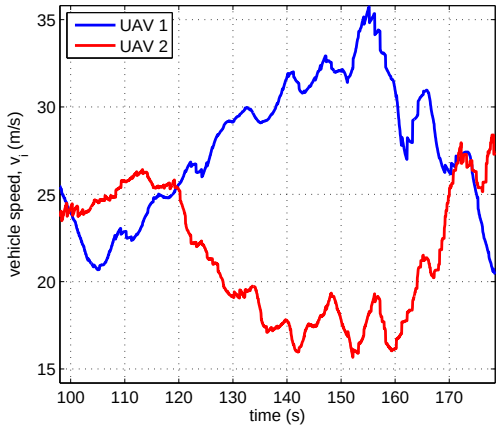

(b) UAV speeds.

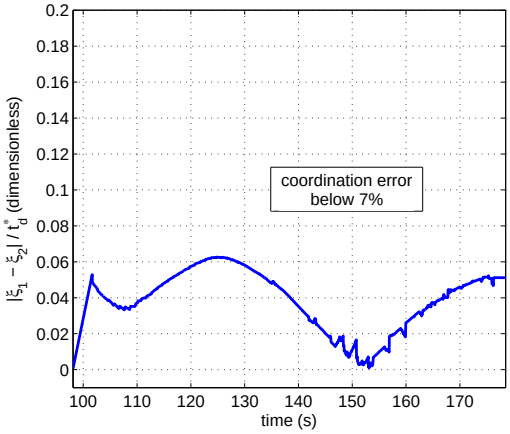

(c) Normalized coordination error.

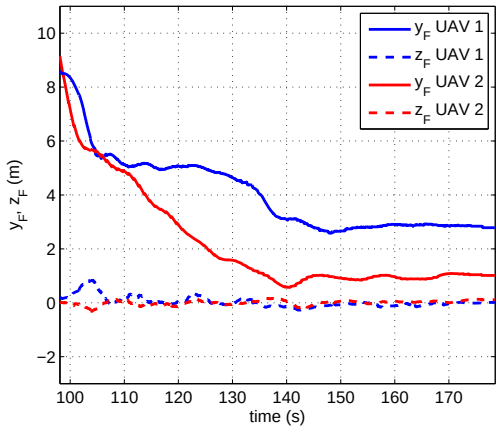

(d) Inter-vehicle separation.

Figure 10. Cooperative path-following control during the road-search phase.

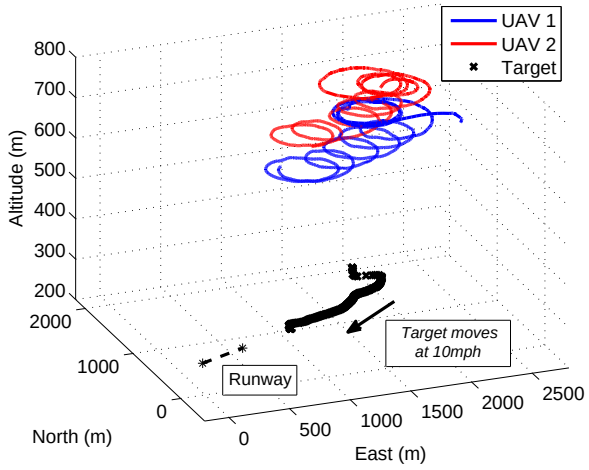

(a) 3D trajectories.

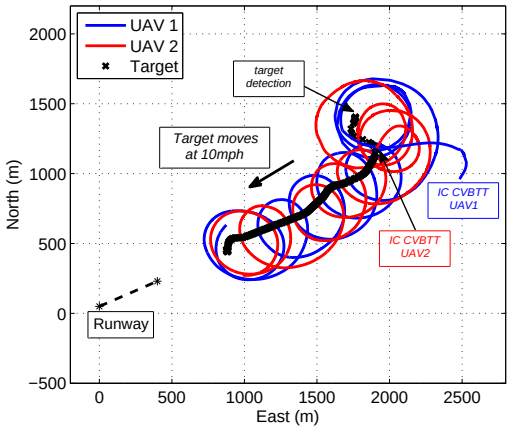

(b) 2D projections.

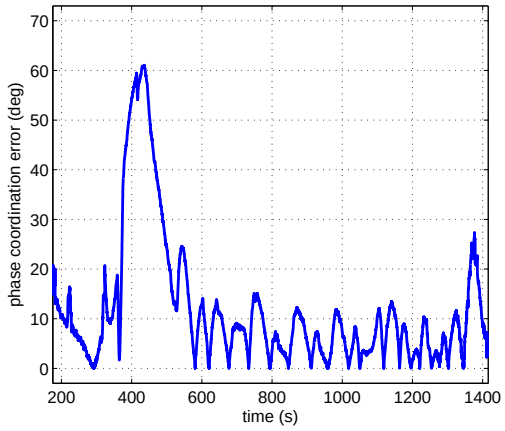

(c) Phase-coordination error.

Figure 11. Cooperative vision-based target tracking (CVBTT).

VII. Conclusions

This paper addressed the problem of multiple Unmanned Aerial Vehicle (UAV) cooperative control in the presence of time-varying communications networks and stringent spatial/temporal constraints. The constraints involve collision-free maneuvers and simultaneous times of arrival at desired target locations (time-critical operations). The methodology proposed in the paper built on previous work by the authors on path following and extended it to a very general setting that allows for the consideration of complex vehicle dynamics, time-critical specifications, and time-varying communications topologies. In the setup adopted, single-vehicle path-following control in 3-D space was done by resorting to a nonlinear control strategy derived at the kinematic level. Decentralized, multiple vehicle time-critical cooperative path following was achieved by adjusting the speed of each vehicle about a nominal speed profile, in response to information exchanged with its neighbors over a dynamic communications network. We addressed explicitly the situation where each vehicle transmits only its coordination state to only a subset of the other vehicles, as determined by the communications topology adopted. Furthermore, we considered the case where the communications graph that captures the underlying communications network topology is be disconnected during some interval of time (or even fails to be connected for the entire duration of the mission) and provided conditions under which the complete coordinated path-following closed-loop system is stable and yields convergence of conveniently defined cooperation error states to a neighborhood of the origin. Flight tests of a coordinated road search mission scenario that exploited the multi-UAV cooperative control framework exposed in the paper demonstrated the efficacy of the algorithms developed. Future work will aim at extending the algorithms presented to other kinds of vehicles and maneuvers; e.g., quadrotor UAVs undergoing complex time-critical maneuvers that require synchronization of attitude and position.

References

[1]Isaac Kaminer, António M. Pascoal, Eric Hallberg, and Carlos Silvestreo. Trajectory tracking for autonomous vehicles: An integrated approach to guidance and control. *Journal of Guidance, Control and Dynamics*, 21(1):29–38, January–February 1998.

[2]Yoonsoo Kim and Mehran Mesbahi. On maximizing the second smallest eigenvalue of state-dependent graph Laplacian. *IEEE Transactions on Automatic Control*, 51(1):116–120, January 2006.

[3]John N. Tsitsiklis and Michael Athans. Convergence and asymptotic agreement in distributed decision problems. *IEEE Transactions on Automatic Control*, 29(1):42–50, January 1984.

[4]Rodolphe Sepulchre, Derek Paley, and Naomi Leonard. *Collective Motion and Oscillator Synchronization*, volume 309 of *Lecture Notes in Control and Information Sciences*, pages 189–206. Springer-Verlag Berlin, 2005.

[5]Ali Jadbabaie, Jie Lin, and A. Stephen Morse. Coordination of groups of mobile autonomous agents using nearest neighbor rules. *IEEE Transactions on Automatic Control*, 48(6):988–1001, June 2003.

[6]Zhiyun Lin, Bruce A. Francis, and Manfredi Maggiore. State agreement for continuous-time coupled nonlinear systems. *SIAM Journal on Control and Optimization*, 46(1):288–307, 2007.

[7]Magnus Egerstedt and Xiaoming Hu. Formation constrained multi-agent control. *IEEE Transactions on Robotics and Automation*, 17(6):947–951, December 2001.

[8]Reza Ghabcheloo, António M. Pascoal, Carlos Silvestre, and Isaac Kaminer. Coordinated path following control of multiple wheeled robots using linearization techniques. *International Journal of Systems Science*, 37(6):399–414, May 2006.

[9]Lei Fang, Panos J. Antsaklis, and Anastasis Tzimas. Asynchronous consensus protocols: Preliminary results, simulations and open questions. In *IEEE Conference on Decision and Control*, pages 2194–2199, Seville, Spain, December 2005.

[10]Mehran Mesbahi. On state-dependent dynamic graphs and their controllability properties. *IEEE Transactions on Automatic Control*, 50(3):387–392, March 2005.

[11]Daniel J. Stilwell and Bradley E. Bishop. Platoons of underwater vehicles. *IEEE Control Systems Magazine*, 20(6):45–52, December 2000.

[12]Daniel J. Stilwell, Erik M. Bollt, and D. Gray Roberson. Sufficient conditions for fast switching synchronization in time-varying network topologies. *SIAM Journal of Applied Dynamical Systems*, 5(1):140–156, 2006.

[13]Ming Cao, Daniel A. Spielman, and A. Stephen Morse. A lower bound on convergence of a distributed network consensus algorithm. In *IEEE Conference on Decision and Control*, pages 2356–2361, Seville, Spain, December 2005.

[14]Mehran Mesbahi and Fred Y. Hadaegh. Formation flying control of multiple spacecraft via graphs, matrix inequalities, and switching. *Journal of Guidance, Control and Dynamics*, 24(2):369–377, March–April 2001.

[15]Yongduan D. Song, Yao Li, and Xiao H. Liao. Orthogonal transformation based robust adaptive close formation control of multi-UAVs. In *American Control Conference*, volume 5, pages 2983–2988, Portland, OR, June 2005.

[16]Dušan M. Stipanović, Gökhan İnalhan, Rodney Teo, and Claire J. Tomlin. Decentralized overlapping control of a formation of unmanned aerial vehicles. *Automatica*, 40(8):1285–1296, August 2004.

[17]Reza Ghabcheloo, A. Pedro Aguiar, António M. Pascoal, Carlos Silvestre, Isaac Kaminer, and João P. Hespanha. Coordinated path-following control of multiple underactuated autonomous vehicles in presence of communication failures. In *IEEE Conference on Decision and Control*, pages 4345–4350, San Diego, CA, December 2006.

[18]F. Lobo Pereira and J. Borges de Sousa. Coordinated control of networked vehicles: An autonomous underwater system. *Automation and Remote Control*, 65(7):1037–1045, July 2004.

[19]Isaac Kaminer, Oleg A. Yakimenko, Vladimir Dobrokhodov, António M Pascoal, Naira Hovakimyan, Vijay V. Patel, Chengyu Cao, and Amanda Young. Coordinated path following for time-critical missions of multiple UAVs via $\mathcal{L}_1$ adaptive output feedback controllers. In *AIAA Guidance, Navigation and Control Conference*, Hilton Head, SC, August 2007. AIAA-2007-6409.

[20]A. P. Aguiar and A. M. Pascoal. Coordinated path-following control for nonlinear systems with logic-based communication. In *Proc. 46h IEEE Conference on Decision and Control*, New Orleans, USA, December 2007.

[21]A. P. Aguiar, I. Kaminer, R. Ghabcheloo, A. M. Pascoal, E. Xargay, N. Hovakimyan, C. Cao, and V. Dobrokhodov. Coordinated path following of multiple uavs for time-critical missions in the presence of time-varying communication topologies. In *Proc. 17th IFAC World Congress*, Seoul, Korea, July 2008.

[22]Reza Ghabcheloo, Isaac Kaminer, A. Pedro Aguiar, and António M. Pascoal. A general framework for multiple vehicle time-coordinated path following control. In *American Control Conference*, pages 3071–3076, St. Louis, MO, June 2009.

[23]R Ghabcheloo, Aguiar A. P, A. Pascoal, C. Silvestre, I. Kaminer, and J. Hespanha. Coordinated path-following in the presence of communication losses and delays. *SIAM Journal on Control and Optimization*, 48(1):234–265, 2009.

[24]Isaac Kaminer, António Pascoal, Enric Xargay, Naira Hovakimyan, Chengyu Cao, and Vladimir Dobrokhodov. Path following for unmanned aerial vehicles using $\mathcal{L}_1$ adaptive augmentation of commercial autopilots. *Journal of Guidance, Control and Dynamics*, 33(2):550–564, March–April 2010.

[25]Roger Skjetne, Sonja Moi, and Thor I. Fossen. Nonlinear formation control of marine craft. In *IEEE Conference on Decision and Control*, volume 2, pages 1699–1704, Las Vegas, NV, December 2002.

[26]Ivar-André F. Ihle. *Coordinated Control of Marine Craft*. PhD thesis, Norwegian University of Science and Technology, Trondheim, Norway, September 2006.

[27]Erik Kyrkjebø. *Motion Coordination of Mechanical Systems: Leader-Follower Synchronization of Euler-Lagrange Systems Using Output Feedback Control*. PhD thesis, Norwegian University of Science and Technology, Trondheim, Norway, April 2007.

[28]F. Arrichiello, S. Chiaverini, and T. I. Fossen. *Formation Control of Marine Surface Vessels using the Null-Space-Based Behavioral Control, in Group Coordination and Cooperative Control, Lecture Notes in Control and Information Systems Series (K. Y. Pettersen, T. Gravdahl, and H. Nijmeijer, Eds.)*. Springer-Verlag, 2006.

[29]M. Breivik, V. Subbotin, and T. I. Fossen. *Kinematic Aspects of Guided Formation Control in 2D, in Group Coordination and Cooperative Control, Lecture Notes in Control and Information Systems Series (K. Y. Pettersen, T. Gravdahl, and H. Nijmeijer, Eds.* Springer-Verlag, 2006.

[30]I. Ihle, J. Jouffroy, and T. I. Fossen. *Robust Formation Control of Marine Craft using Lagrange Multipliers, in Group Coordination and Cooperative Control, Lecture Notes in Control and Information Systems Series (K. Y. Pettersen, T. Gravdahl, and H. Nijmeijer, Eds.)*. Springer-Verlag, 2006.

[31]M. Breivik, E. Hovstein, and T. I. Fossen. Ship formation control: A guided leader-follower approach. In *Proc. IFAC World Congress*, Seoul, Korea, 2008.

[32]Thor I. Fossen. *Marine Control Systems: Guidance, Navigation and Control of Ships, Rigs and Underwater Vehicles*. Marine Cybernetics, Norway, 2002.

[33]Y. Xu and J. P. Hespanha. *Communication logic design and analysis for networked control systems. In Current trends in nonlinear systems and control (L. Menini,L. Zaccarian, and C. T. Abdallah, Eds.)*. Birkhauser, Boston, 2006.

[34]J. K. Yook, D. M. Tilbury, and N. R. Soparkar. Trading computation for bandwidth: Reducing communication in distributed control systems using state estimators. *IEEE Trans. Contr. Syst. Technol*, 10(3):503–518, 2002.

[35]Enric Xargay, Vladimir Dobrokhodov, Isaac Kaminer, António M. Pascoal, Naira Hovakimyan, and Chengyu Cao. Cooperative control of autonomous systems. Accepted for publication to *IEEE Control Systems Magazine*, 2011.

[36]Alain Micaelli and Claude Samson. Trajectory tracking for unicycle-type and two-steering-wheels mobile robot. Technical Report 2097, INRIA, Sophia-Antipolis, France, November 1993.

[37]Didik Soetanto, Lionel Lapierre, and António M. Pascoal. Adaptive, non-singular path-following control of dynamic wheeled robots. In *International Conference on Advanced Robotics*, pages 1387–1392, Coimbra, Portugal, June–July 2003.

[38]Richard L. Bishop. There is more than one way to frame a curve. *The American Mathematical Monthly*, 82(3):246–251, 1975.

[39]Andrew J. Hanson and Hui Ma. Parallel transport approach to curve framing. Technical report, Indiana University Compute Science Department, 1995.

[40]Norman Biggs. *Algebraic Graph Theory*. Cambridge University Press, New York, NY, 1993.

[41]Murat Arcak. Passivity as a design tool for group coordination. *IEEE Transactions on Automatic Control*, 52(8):1380–1390, August 2007.

[42]Vladimir Dobrokhodov, Isaac Kaminer, Ioannis Kitsios, Enric Xargay, Naira Hovakimyan, Chengyu Cao, Irene M. Gregory, and Lena Valavani. Experimental validation of $\mathcal{L}_1$ adaptive control: Rohrs' counterexample in flight. *Journal of Guidance, Control and Dynamics*, 2011. Accepted for publication.

[43]Taeyoung Lee, Melvin Leok, and N. Harris McClamroch. Control of complex maneuvers for a quadrotor UAV using geometric methods on $\mathsf{SE}(3)$. *IEEE Transactions on Automatic Control*, 2010. Submitted. Available online: `arXiv:1003.2005v3`.

[44]Venanzio Cichella, Enric Xargay, Vladimir Dobrokhodov, Isaac Kaminer, António M. Pascoal, and Naira Hovakimyan. Geometric 3D path-following control for a fixed-wing UAV on $\mathsf{SO}(3)$. In *AIAA Guidance, Navigation and Control Conference*, Portland, OR, August 2011. AIAA-2011-6415.

[45]Evgeny Kharisov, Xiaofeng Wang, and Naira Hovakimyan. Distributed event-triggered consensus algorithm for uncertain multi-agent systems. In *AIAA Guidance, Navigation and Control Conference*, Toronto, Canada, August 2010. AIAA-2010-8325.

[46]A. Pedro Aguiar, Isaac Kaminer, Reza Ghabcheloo, António M. Pascoal, Enric Xargay, Naira Hovakimyan, Chengyu Cao, and Vladimir Dobrokhodov. Time-coordinated path following of multiple UAVs over time-varying networks using $\mathcal{L}_1$ adaptation. In *AIAA Guidance, Navigation and Control Conference*, Honolulu, HI, August 2008. AIAA-2008-7131.

[47]PC104-Plus Embedded Single Board Computers: AMD Geode LX800 CPU 500MHz - MSM800SEV/SEL/BEV.

[48]Persistent Systems: Wave Relay. http://www.persistentsystems.com.

[49]J. Burl. Piccolo/Piccolo Plus Autopilots - Highly Integrated Autopilots for Small UAVs. http://cloudcaptech.com.

[50]Michael R. Clement, Eugene Bourakov, Kevin D. Jones, and Vladimir Dobrokhodov. Exploring network-centric information architectures for unmanned systems control and data dissemination. In *AIAA Infotech@Aerospace*, Seattle, WA, April 2009. AIAA-2009-1999.

[51]Michael T. Flynn, Rich Juergens, and Thomas L. Cantrell. Employing ISR: SOF best practices. *Joint Force Quarterly*, 50:56–61, July 2008.

[52]Vladimir Dobrokhodov, Isaac Kaminer, Kevin D. Jones, and Reza Ghabcheloo. Vision-based tracking and motion estimation for moving targets using small UAVs. *Journal of Guidance, Control and Dynamics*, 31(4):907–917, July–August 2008.

[53]Stephen Morris and Eric W. Frew. Cooperative tracking of moving targets by teams of autonomous unmanned air vehicles. Technical Report FA9550-04-C-0107, MLB Company and University of Colorado, July 2004.

[54]2d3, Applications. http://www.2d3.com/application, May 2010.

[55]Hassan K. Khalil. *Nonlinear Systems*. Prentice Hall, Englewood Cliffs, NJ, 2002.

[56]Antonio Loría and Elena Panteley. Uniform exponential stability of linear time-varying systems: Revisited. *Systems & Control Letters*, 47(1):13–24, September 2002.

[57]Elena Panteley and Antonio Loría. Uniform exponential stability for families of linear time-varying systems. In *IEEE Conference on Decision and Control*, pages 1948–1953, Sydney, Australia, December 2000.

Appendix

A. The *hat* and *vee* maps [43]

The *hat map* $(\cdot)^\wedge : \mathbb{R}^3 \to \mathsf{SO}(3)$ is defined as

$$(x)^\wedge = \begin{bmatrix} 0 & -x_3 & x_2 \\ x_3 & 0 & -x_1 \\ -x_2 & x_1 & 0 \end{bmatrix}$$

for $x = [x_1,\ x_2,\ x_3]^\top \in \mathbb{R}^3$. The inverse of the hat map is referred to as the *vee map* $(\cdot)^\vee : \mathsf{SO}(3) \to \mathbb{R}^3$. A property of the hat and vee maps used in this paper is given below:

$$\mathrm{tr}\left[M(x)^\wedge\right] = -x \cdot \left(M - M^\top\right)^\vee , \tag{45}$$

for any $x \in \mathbb{R}^3$, and $M \in \mathbb{R}^{3\times 3}$. We refer to [43] for further details on the hat and vee maps.

B. Proof of Lemma 1

We start by noting that over the compact set Ω_c introduced in (20) the following upper bounds hold:

$$\|p_F\| \le cc_1 < \frac{c_1}{\sqrt{2}}, \tag{46}$$

$$\Psi(\tilde{R}) \le c^2 < \frac{1}{2}. \tag{47}$$

Consider now the Lyapunov function candidate

$$V_{pf}(p_F, \tilde{R}) = \Psi(\tilde{R}) + \frac{1}{c_1^2}\|p_F\|^2 .$$

This function is locally positive-definite about $(p_F, \tilde{R}_{11}) = (0, 1)$ within the region Ω_c defined in (20). Moreover, we note that $\|e_{\tilde{R}}\|$ can be related to the function $\Psi(\tilde{R})$ as follows:

$$\|e_{\tilde{R}}\|^2 = \frac{1}{4}\left(\tilde{R}_{12}^2 + \tilde{R}_{13}^2\right) = \frac{1}{4}\left(1 - \tilde{R}_{11}^2\right) = \frac{1}{4}\left(1 - \tilde{R}_{11}\right)\left(1 + \tilde{R}_{11}\right) = \Psi(\tilde{R})\left(1 - \Psi(\tilde{R})\right) .$$

Then, the bound in (47) implies that, inside the set Ω_c, the Lyapunov function V_{pf} can be bounded as

$$\|e_{\tilde{R}}\|^2 + \frac{1}{c_1^2}\|p_F\|^2 \le V_{pf} \le \frac{1}{1-c^2}\|e_{\tilde{R}}\|^2 + \frac{1}{c_1^2}\|p_F\|^2 . \tag{48}$$

From equations (1) and (5), the time derivative of V_{pf} is given by

$$\dot{V}_{pf} = e_{\tilde{R}} \cdot \left(\begin{bmatrix} q \\ r \end{bmatrix} - \Pi_R \tilde{R}^\top \left(R_F^D \{\omega_{F/I}\}_F + \{\omega_{D/F}\}_D \right) \right) + \frac{2}{c_1^2} p_F \cdot \left(-\dot{\ell}\, \vec{t} - \omega_{F/I} \times p_F + v\, \vec{w}_1 \right) .$$

The rate commands (15), together with the law (14) for the rate of progression of the virtual target along the path, lead to

$$\dot{V}_{pf} = -2K_{\tilde{R}}\, e_{\tilde{R}} \cdot e_{\tilde{R}} + \frac{2}{c_1^2} \left(-K_\ell \left(p_F \cdot \vec{t} \right)^2 - p_F \cdot \left(\omega_{F/I} \times p_F \right) + v\, p_F \cdot \left(\vec{w}_1 - \left(\vec{w}_1 \cdot \vec{t} \right) \vec{t} \right) \right) . \tag{49}$$

Since $\left(p_F \cdot \vec{t} \right) = x_F$ and, moreover, we have that $\left(p_F \cdot \left(\omega_{F/I} \times p_F \right) \right) = 0$, then (49) reduces to

$$\dot{V}_{pf} = -2K_{\tilde{R}}\, e_{\tilde{R}} \cdot e_{\tilde{R}} - \frac{2K_\ell}{c_1^2} x_F^2 + \frac{2v}{c_1^2} \left(p_F \cdot \left(\vec{w}_1 - \left(\vec{w}_1 \cdot \vec{t} \right) \vec{t} \right) \right) . \tag{50}$$

Letting $p_\times(t)$ denote the cross-track error, which can be expressed as

$$p_\times = \left(p_F \cdot \vec{n}_1 \right) \vec{n}_1 + \left(p_F \cdot \vec{n}_2 \right) \vec{n}_2 = y_F\, \vec{n}_1 + z_F\, \vec{n}_2 , \tag{51}$$

we have the following equality:

$$p_F \cdot \left(\vec{w}_1 - \left(\vec{w}_1 \cdot \vec{t} \right) \vec{t} \right) = p_F \cdot \left(\left(\vec{w}_1 \cdot \vec{n}_1 \right) \vec{n}_1 + \left(\vec{w}_1 \cdot \vec{n}_2 \right) \vec{n}_2 \right) = p_\times \cdot \vec{w}_1 . \tag{52}$$

Substituting (52) into (50), we obtain

$$\dot{V}_{pf} = -2K_{\tilde{R}}\, e_{\tilde{R}} \cdot e_{\tilde{R}} - \frac{2K_\ell}{c_1^2} x_F^2 + \frac{2v}{c_1^2} \left(p_\times \cdot \vec{w}_1 \right) . \tag{53}$$

Consider now the quantity $\left(\vec{w}_1 \cdot \vec{b}_{1D} \right)$, which represents the cosine of the angle ψ_e between the desired direction of the velocity vector $\vec{b}_{1D}$ and the actual direction of the UAV's velocity vector $\vec{w}_1$. From the definition of $\Psi(\tilde{R})$ in (3), we have that

$$\vec{w}_1 \cdot \vec{b}_{1D} = \cos \psi_e = \tilde{R}_{11} = 1 - 2\Psi(\tilde{R}) .$$

The bound in (47) implies that, within the set Ω_c, the quantity $\left(\vec{w}_1 \cdot \vec{b}_{1D} \right)$ is bounded away from zero:

$$\vec{w}_1 \cdot \vec{b}_{1D} = 1 - 2\Psi(\tilde{R}) \geq 1 - 2c^2 > 0 .$$

The quantity $\frac{1}{\left(\vec{w}_1 \cdot \vec{b}_{1D} \right)}$ is therefore well defined within the set Ω_c. Next, we add and subtract the term $\frac{2v}{c_1^2} \frac{\left(p_\times \cdot \vec{b}_{1D} \right)}{\left(\vec{w}_1 \cdot \vec{b}_{1D} \right)}$ to (53) to obtain

$$\dot{V}_{pf} = -2K_{\tilde{R}}\, e_{\tilde{R}} \cdot e_{\tilde{R}} - \frac{2K_\ell}{c_1^2} x_F^2 + \frac{2v}{c_1^2} \frac{\left(p_\times \cdot \vec{b}_{1D} \right)}{\left(\vec{w}_1 \cdot \vec{b}_{1D} \right)} + \frac{2v}{c_1^2} \frac{p_\times \cdot \left(\vec{w}_1 \times \left(\vec{w}_1 \times \vec{b}_{1D} \right) \right)}{\left(\vec{w}_1 \cdot \vec{b}_{1D} \right)} .$$

The definitions of $\vec{b}_{1D}(t)$ and $p_\times(t)$ in (2) and (51) lead to

$$\dot{V}_{pf} = -2K_{\tilde{R}}\, e_{\tilde{R}} \cdot e_{\tilde{R}} - \frac{2K_\ell}{c_1^2} x_F^2 - \frac{2v}{c_1^2 \left(\vec{w}_1 \cdot \vec{b}_{1D} \right) \left(d^2 + p_\times \cdot p_\times \right)^{\frac{1}{2}}} p_\times \cdot p_\times + \frac{2v}{c_1^2} \frac{p_\times \cdot \left(\vec{w}_1 \times \left(\vec{w}_1 \times \vec{b}_{1D} \right) \right)}{\left(\vec{w}_1 \cdot \vec{b}_{1D} \right)} .$$

Next, we note that, within the set Ω_c, the following bounds hold:

$$0 < 1 - 2c^2 \leq \left(\vec{w}_1 \cdot \vec{b}_{1D} \right) \leq 1 , \qquad \| p_\times \| \leq \| p_F \| \leq c c_1 .$$

These bounds, together with the assumption on the UAV speed in (16), yield the following bound for $\dot{V}_{pf}$:

$$\dot{V}_{pf} \leq -2K_{\tilde{R}} \| e_{\tilde{R}} \|^2 - \frac{2K_\ell}{c_1^2} x_F^2 - \frac{2v_{\min}}{c_1^2 \left(d^2 + c^2 c_1^2 \right)^{\frac{1}{2}}} \| p_\times \|^2 + \frac{2v_{\max}}{c_1^2 (1 - 2c^2)} \| p_\times \| \, \| \vec{w}_1 \times \left(\vec{w}_1 \times \vec{b}_{1D} \right) \| .$$

The term $\| \vec{w}_1 \times \left(\vec{w}_1 \times \vec{b}_{1D} \right) \|$ represents the absolute value of the sine of the angle ψ_e. Therefore, we can write

$$\| \vec{w}_1 \times \left(\vec{w}_1 \times \vec{b}_{1D} \right) \| = |\sin(\psi_e)| = \sqrt{1 - \cos^2(\psi_e)} = \sqrt{1 - \tilde{R}_{11}^2} = \sqrt{\tilde{R}_{12}^2 + \tilde{R}_{13}^2} = 2 \| e_{\tilde{R}} \| ,$$

which yields

$$\dot{V}_{pf} \leq -2K_{\tilde{R}} \| e_{\tilde{R}} \|^2 - \frac{2K_\ell}{c_1^2} x_F^2 - \frac{2v_{\min}}{c_1^2 \left(d^2 + c^2 c_1^2 \right)^{\frac{1}{2}}} \| p_\times \|^2 + \frac{4v_{\max}}{c_1^2 (1 - 2c^2)} \| p_\times \| \, \| e_{\tilde{R}} \| .$$

Letting $K_p \triangleq \min\left\{K_\ell\,,\ \frac{v_{\min}}{(d^2+c^2c_1^2)^{\frac{1}{2}}}\right\}$ and noting that $\|p_\times\| \leq \|p_F\|$, we have

$$\dot{V}_{pf} \leq -2K_{\tilde{R}}\|e_{\tilde{R}}\|^2 - \frac{2K_p}{c_1^2}\|p_F\|^2 + \frac{4v_{\max}}{c_1^2(1-2c^2)}\|p_F\|\,\|e_{\tilde{R}}\|\,.$$

From the choice for the characterizing distance d and the path-following control parameters K_ℓ and $K_{\tilde{R}}$ in (17) and the definition of λ_{pf}^* in (19), it follows that:

$$\begin{bmatrix} K_{\tilde{R}} & -\frac{v_{\max}}{c_1^2(1-2c^2)} \\ -\frac{v_{\max}}{c_1^2(1-2c^2)} & \frac{K_p}{c_1^2} \end{bmatrix} \geq \lambda_{pf}^* \begin{bmatrix} \frac{1}{1-c^2} & 0 \\ 0 & \frac{1}{c_1^2} \end{bmatrix},$$

which implies that, within the set Ω_c, the following bound holds:

$$\dot{V}_{pf} \leq -2\lambda_{pf}^*\left(\frac{1}{1-c^2}\|e_{\tilde{R}}\|^2 + \frac{1}{c_1^2}\|p_F\|^2\right) \leq -2\lambda_{pf}^* V_{pf}\,.$$

It follows from [55, Theorem 4.10] that both $\|e_{\tilde{R}}\|$ and $\|p_F\|$ converge exponentially to zero for all the initial conditions inside the compact set Ω_c. □

C. Proof of Lemma 2

First, we show that the rate commands $q_c(t)$ and $r_c(t)$ are bounded for all $(p_F, e_{\tilde{R}}) \in \Omega_c$. Over the compact set Ω_c, which was introduced in (20), the following inequalities hold:

$$\|p_F\| \leq cc_1\,, \tag{54}$$
$$\Psi(\tilde{R}) \leq c^2\,. \tag{55}$$

The first inequality above, together with the bound on the UAV speed in (16), implies that $\dot{\ell}(t)$ satisfies

$$|\dot{\ell}| \leq v_{\max} + K_\ell\, cc_1\,.$$

From the assumption on the feasibility of the path, we can conclude that both parameters $k_1(\ell)$ and $k_2(\ell)$ are bounded, and therefore the bound on $\dot{\ell}(t)$ implies that $\omega_{F/I}(t)$ is also bounded. It then follows from (6) that $\dot{p}_F$ is bounded, which, along with the inequality in (54), implies that the entries of $\dot{R}_D^F(t)$ are bounded. From the kinematic equation

$$\left(\{\omega_{D/F}\}_D\right)^\wedge = R_F^D\dot{R}_D^F\,,$$

it follows that $\omega_{D/F}(t)$ is also bounded. Moreover, (55) implies that the attitude error $e_{\tilde{R}}(t)$ satisfies

$$\|e_{\tilde{R}}\| \leq c^2\,.$$

From the bounds on $\omega_{F/I}(t)$, $\omega_{D/F}(t)$, and $e_{\tilde{R}}(t)$ it follows that, for all $(p_F, e_{\tilde{R}}) \in \Omega_c$, the rate commands $q_c(t)$ and $r_c(t)$ are bounded. Then, based on the assumption made in Section II.C on the tracking capabilities of the UAV with its autopilot, we have that, for all $(p_F, e_{\tilde{R}}) \in \Omega_c$, the following performance bounds hold:

$$|q_c - q| \leq \gamma_q\,, \tag{56a}$$
$$|r_c - r| \leq \gamma_r\,. \tag{56b}$$

Next, we consider again the Lyapunov function candidate

$$V_{pf}(p_F, \tilde{R}) = \Psi(\tilde{R}) + \frac{1}{c_1^2}\|p_F\|^2\,.$$

From equations (1) and (5), the time derivative of V_{pf} is given by

$$\dot{V}_{pf} = e_{\tilde{R}} \cdot \left(\begin{bmatrix} q \\ r \end{bmatrix} - \Pi_R\tilde{R}^\top\left(R_F^D\{\omega_{F/I}\}_F + \{\omega_{D/F}\}_D\right)\right) + \frac{2}{c_1^2}p_F \cdot \left(-\dot{\ell}\,\vec{t} - \omega_{F/I}\times p_F + v\,\vec{w}_1\right).$$

We add and subtract the term $e_{\tilde{R}} \cdot \left[\begin{smallmatrix} q_c \\ r_c \end{smallmatrix}\right]$ to the above equation to obtain

$$\dot{V}_{pf} = e_{\tilde{R}} \cdot \left(\begin{bmatrix} q_c \\ r_c \end{bmatrix} - \Pi_R\tilde{R}^\top\left(R_F^D\{\omega_{F/I}\}_F + \{\omega_{D/F}\}_D\right)\right) + \frac{2}{c_1^2}p_F \cdot \left(-\dot{\ell}\,\vec{t} - \omega_{F/I}\times p_F + v\,\vec{w}_1\right) - e_{\tilde{R}} \cdot \begin{bmatrix} q_c - q \\ r_c - r \end{bmatrix}.$$

Similar to the proof of Lemma 1, we have that, inside the set Ω_c, the following bound holds:

$$\dot{V}_{pf} \leq -2\lambda^*_{pf}\left(\frac{1}{1-c^2}\left\|e_{\tilde{R}}\right\|^2 + \frac{1}{c_1^2}\left\|p_F\right\|^2\right) + \left\|e_{\tilde{R}}\right\|\left\|\begin{bmatrix} q_c - q \\ r_c - r \end{bmatrix}\right\|,$$

where λ^*_{pf} was defined in (19). From the performance bounds in (56) and the definition of γ_ω in (22), it follows that

$$\left\|\begin{bmatrix} q_c - q \\ r_c - r \end{bmatrix}\right\| \leq \gamma_\omega\,,$$

which leads to

$$\dot{V}_{pf} \leq -2\lambda^*_{pf}\left(\frac{1}{1-c^2}\left\|e_{\tilde{R}}\right\|^2 + \frac{1}{c_1^2}\left\|p_F\right\|^2\right) + \left\|e_{\tilde{R}}\right\|\gamma_\omega\,.$$

We now rewrite the above inequality as

$$\dot{V}_{pf} \leq -2(\lambda^*_{pf} - \delta_\lambda)\left(\frac{1}{1-c^2}\left\|e_{\tilde{R}}\right\|^2 + \frac{1}{c_1^2}\left\|p_F\right\|^2\right) - 2\delta_\lambda\left(\frac{1}{1-c^2}\left\|e_{\tilde{R}}\right\|^2 + \frac{1}{c_1^2}\left\|p_F\right\|^2\right) + \left\|e_{\tilde{R}}\right\|\gamma_\omega\,,$$

where $0 < \delta_\lambda < \lambda^*_{pf}$. Then, for all $p_F(t)$ and $e_{\tilde{R}}(t)$ satisfying

$$-2\delta_\lambda\left(\frac{1}{1-c^2}\left\|e_{\tilde{R}}\right\|^2 + \frac{1}{c_1^2}\left\|p_F\right\|^2\right) + \left\|e_{\tilde{R}}\right\|\gamma_\omega \leq 0\,, \tag{57}$$

we have

$$\dot{V}_{pf} \leq -2(\lambda^*_{pf} - \delta_\lambda)\left(\frac{1}{1-c^2}\left\|e_{\tilde{R}}\right\|^2 + \frac{1}{c_1^2}\left\|p_F\right\|^2\right) \leq -2(\lambda^*_{pf} - \delta_\lambda)V_{pf}\,.$$

The inequality in (57) is satisfied outside the bounded set D defined by:

$$D \triangleq \left\{(p_F, \tilde{R}) \in \mathbb{R}^3 \times \mathsf{SO(3)} \mid \frac{1}{1-c^2}\left(\left\|e_{\tilde{R}}\right\| - \frac{(1-c^2)\,\gamma_\omega}{4\delta_\lambda}\right)^2 + \frac{1}{c_1^2}\|p_F\|^2 < \frac{(1-c^2)\,\gamma_\omega^2}{16\delta_\lambda^2}\right\}.$$

The set D is in the interior of the compact set F given by:

$$F \triangleq \left\{(p_F, \tilde{R}) \in \mathbb{R}^3 \times \mathsf{SO(3)} \mid \frac{1}{1-c^2}\left\|e_{\tilde{R}}\right\|^2 + \frac{1}{c_1^2}\|p_F\|^2 \leq \frac{(1-c^2)\,\gamma_\omega^2}{4\delta_\lambda^2}\right\},$$

which in its turn is contained in the compact set Ω_b defined by:

$$\Omega_b \triangleq \left\{(p_F, \tilde{R}) \in \mathbb{R}^3 \times \mathsf{SO(3)} \mid \Psi(\tilde{R}) + \frac{1}{c_1^2}\|p_F\|^2 \leq \frac{(1-c^2)\gamma_\omega^2}{4\delta_\lambda^2}\right\}.$$

Then, the design constraint for the performance bounds γ_q and γ_r in (22) implies that the set Ω_b is in the interior of the set Ω_c introduced in (20), that is, $\Omega_b \subset \Omega_c$.

With the above results and using a proof similar to that of Theorem 4.18 in [55], it can be shown that, for every initial state $(p_F(0), \tilde{R}(0)) \in \Omega_c$, there is a time $T_b \geq 0$ such that the following bounds are satisfied:

$$V_{pf}(t) \leq V_{pf}(0)\mathrm{e}^{-2(\lambda^*_{pf} - \delta_\lambda)t}\,, \qquad \forall\ 0 \leq t < T_b\,,$$
$$V_{pf}(t) \leq \frac{(1-c^2)\gamma_\omega^2}{4\delta_\lambda^2}\,, \qquad \forall\ t \geq T_b\,.$$

The bounds in (23) and (24) follow immediately from the two bounds above and the inequalities in (48). □

D. Proof of Lemma 3

To prove ISS we first show that the homogeneous equation of the coordination dynamics

$$\dot{\zeta}(t) = F(t)\zeta(t) \tag{58}$$

is globally uniformly exponentially stable (GUES). To this end, we first consider the system

$$\dot{\phi}(t) = -a\bar{L}(t)\phi(t)\,, \tag{59}$$

where a is the proportional coordination control gain introduced in (28). Letting $D(t)$ be the time-varying incidence matrix, $L(t) = D(t)\,D^\top(t)$, we can rewrite the above system as:

$$\dot{\phi}(t) = -a(QD(t))(QD(t))^\top\phi(t)\,.$$

Then, since $QD(t)$ is piecewise-constant and in addition we have that

$$\|QD(t)\|^2 \leq n\,,$$

one can prove that the system in (59) is GUES, and the following bound holds:

$$\|\phi(t)\| \leq k_\lambda \,\|\phi(0)\|\, \mathrm{e}^{-\gamma_\lambda t}$$

with

$$k_\lambda = 1\,, \qquad \text{and} \qquad \gamma_\lambda \geq \bar{\gamma}_\lambda \triangleq \frac{an\mu}{(1+anT)^2}\,.$$

This result can be proven along the same lines as Lemma 5 in [56] or Lemma 3 in [57]. Since $\bar{L}(t)$ is continuous for almost all $t \geq 0$ and uniformly bounded, and the system (59) is GUES, Lemma 1 in [57] and a similar argument as in [55, Theorem 4.12] imply that, for any $\bar{c}_3$ and $\bar{c}_4$ satisfying $0 < \bar{c}_3 \leq \bar{c}_4$, there exists $P_{c_0}(t) = P_{c_0}^\top(t)$, such that

$$\underbrace{\frac{\bar{c}_3}{2an}}_{\triangleq \bar{c}_1}\mathbb{I}_{n-1} \;\leq\; P_{c_0}(t) \;\leq\; \underbrace{\frac{\bar{c}_4}{2\gamma_\lambda}}_{\triangleq \bar{c}_2}\mathbb{I}_{n-1}\,, \tag{60}$$

$$\dot{P}_{c_0}(t) - a\bar{L}(t)P_{c_0}(t) - aP_{c_0}(t)\bar{L}(t) \;\leq\; -\,\bar{c}_3\mathbb{I}_{n-1}\,. \tag{61}$$

Next, we apply the similarity transformation

$$z(t) = S_\zeta \zeta(t) = \begin{bmatrix} \mathbb{I}_{n-1} & 0 \\ -\frac{b}{a}C^\top Q^\top & \mathbb{I}_{n-1} \end{bmatrix} \zeta(t)\,, \tag{62}$$

to the original homogeneous system (58), which leads to

$$\dot{z}(t) = S_\zeta F(t) S_\zeta^{-1} z(t) = \begin{bmatrix} -a\bar{L}(t) + \frac{b}{a}QCC^\top Q^\top & QC \\ -\frac{b^2}{a^2}C^\top Q^\top QCC^\top Q^\top & -\frac{b}{a}C^\top Q^\top QC \end{bmatrix} z(t) \tag{63}$$

Consider now the Lyapunov function candidate

$$V_c(t,z) \triangleq z^\top P_c(t)\, z\,,$$

where $P_c(t)$ is defined as

$$P_c(t) \triangleq \begin{bmatrix} P_{c_0}(t) & 0 \\ 0 & \frac{a^3}{b^3}n\,\mathbb{I}_{n-1} \end{bmatrix}.$$

The time derivative of V_c along the trajectories of the system (63) is given by

$$\dot{V}_c(t) = z^\top(t) \begin{bmatrix} \dot{P}_{c_0}(t) - a\bar{L}(t)P_{c_0}(t) - aP_{c_0}(t)\bar{L}(t) + \frac{b}{a}QCC^\top Q^\top P_{c_0}(t) + \frac{b}{a}P_{c_0}(t)QCC^\top Q^\top & P_{c_0}(t)QC - \frac{a}{b}nQCC^\top Q^\top QC \\ C^\top Q^\top P_{c_0}(t) - \frac{a}{b}nC^\top Q^\top QCC^\top Q^\top & -2\frac{a^2}{b^2}nC^\top Q^\top QC \end{bmatrix} z(t)\,.$$

The inequality in (61) implies that

$$\dot{V}_c(t) \leq z^\top(t) \begin{bmatrix} -\bar{c}_3\mathbb{I}_{n-1} + \frac{b}{a}QCC^\top Q^\top P_{c_0}(t) + \frac{b}{a}P_{c_0}(t)QCC^\top Q^\top & P_{c_0}(t)QC - \frac{a}{b}nQCC^\top Q^\top QC \\ C^\top Q^\top P_{c_0}(t) - \frac{a}{b}nC^\top Q^\top QCC^\top Q^\top & -2\frac{a^2}{b^2}nC^\top Q^\top QC \end{bmatrix} z(t)\,.$$

Now, letting

$$a > 0\,, \qquad \lambda_c = \frac{\gamma_\lambda}{2n\sqrt{n}+1}\,, \qquad b = 2a\lambda_c n\,, \qquad \bar{c}_3 = \bar{c}_4 = \frac{\gamma_\lambda}{\lambda_c}\left(\frac{\gamma_\lambda}{\lambda_c} - 1\right)\frac{1}{2n^2}\,, \tag{64}$$

and noting that $\|QC\| = 1$ and $\lambda_{\min}(C^\top Q^\top QC) = \frac{1}{n}$, one can use Schur complements to prove that the inequality

$$\begin{bmatrix} -\bar{c}_3\mathbb{I}_{n-1} + \frac{b}{a}QCC^\top Q^\top P_{c_0}(t) + \frac{b}{a}P_{c_0}(t)QCC^\top Q^\top & P_{c_0}(t)QC - \frac{a}{b}nQCC^\top Q^\top QC \\ C^\top Q^\top P_{c_0}(t) - \frac{a}{b}nC^\top Q^\top QCC^\top Q^\top & -2\frac{a^2}{b^2}nC^\top Q^\top QC \end{bmatrix}$$
$$\leq -2\lambda_c \begin{bmatrix} \bar{c}_2\mathbb{I}_{n-1} & 0 \\ 0 & \frac{a^3}{b^3}n^2C^\top Q^\top QC \end{bmatrix}$$

holds for all $t \geq 0$. Then, for the choice of parameters in (64), the inequality above implies that

$$\dot{V}_c(t) \leq -2\lambda_c\, z^\top(t) \begin{bmatrix} \bar{c}_2\mathbb{I}_{n-1} & 0 \\ 0 & \frac{a^3}{b^3}n^2C^\top Q^\top QC \end{bmatrix} z(t)\,,$$

which, along with the fact that $P_{c_0}(t) \leq \bar{c}_2 \mathbb{I}_{n-1}$ and $\lambda_{\min}(C^\top Q^\top Q C) = \frac{1}{n}$, leads to

$$\dot{V}_c(t) \leq -2\lambda_c \, z^\top(t) \begin{bmatrix} P_{c_0}(t) & 0 \\ 0 & \frac{a^3}{b^3} n \mathbb{I}_{n-1} \end{bmatrix} z(t) = -2\lambda_c \, V_c(t) \, .$$

Application of the comparison lemma (see [55, Lemma 3.4]) leads to the following upper bound:

$$V_c(t) \leq V_c(0) \mathrm{e}^{-2\lambda_c t} \, ,$$

and since $\min\{\bar{c}_1, \frac{a^3}{b^3} n\} \|z(t)\|^2 \leq V_c(t) \leq \max\{\bar{c}_2, \frac{a^3}{b^3} n\} \|z(t)\|^2$, we find that

$$\|z(t)\| \leq \left(\frac{\max\{\bar{c}_2, \frac{a^3}{b^3} n\}}{\min\{\bar{c}_1, \frac{a^3}{b^3} n\}} \right)^{\frac{1}{2}} \|z(0)\| \, \mathrm{e}^{-\lambda_c t} \, .$$

The similarity transformation in (62) implies that

$$\|\zeta(t)\| \leq \|S_\zeta^{-1}\| \left(\frac{\max\{\bar{c}_2, \frac{a^3}{b^3} n\}}{\min\{\bar{c}_1, \frac{a^3}{b^3} n\}} \right)^{\frac{1}{2}} \|S_\zeta\| \, \|\zeta(0)\| \, \mathrm{e}^{-\lambda_c t} \, ,$$

and consequently the system (58) is GUES. Moreover, since $\gamma_\lambda \geq \bar{\gamma}_\lambda$, we have that

$$\lambda_c = \frac{\gamma_\lambda}{2n\sqrt{n}+1} \geq \frac{\bar{\gamma}_\lambda}{2n\sqrt{n}+1} = \frac{an\mu}{(1+anT)^2} \frac{1}{2n\sqrt{n}+1} \triangleq \bar{\lambda}_c \, .$$

We conclude that the forced system (30) is ISS because it is a linear system, the Laplacian $L(t)$ is bounded, the homogeneous equation is GUES, and the speed tracking error vector $e_v(t)$ is assumed to be bounded for all $t \geq 0$. This implies that the bound in (31) holds. The constants k_1 and k_2 in (31) can be derived from a proof similar to those of Theorem 4.19 and Lemma 4.6 in [55].

To prove inequalities (32) and (33), we introduce the *disagreement vector* $\varrho(t) \triangleq \Pi \, \xi(t)$ and use the facts that

$$\xi_i(t) - \xi_j(t) = \varrho_i(t) - \varrho_j(t) \qquad i = 1, 2, \ldots, n; \quad j = 1, 2, \ldots, n \, , \tag{65}$$

$$\|\varrho(t)\| = \|\zeta_1(t)\| \, , \tag{66}$$

$$\zeta_{2,i}(t) = \chi_{I,i}(t) - 1 \qquad i = 2, \ldots, n \, . \tag{67}$$

It follows from the relationships (65) and (66) that

$$|\xi_i(t) - \xi_j(t)| \;=\; |\varrho_i(t) - \varrho_j(t)| \;\leq\; |\varrho_i(t)| + |\varrho_j(t)| \;\leq\; 2\|\varrho(t)\| \;=\; 2\|\zeta_1(t)\| \, ,$$

and thus equation (31) leads to (32) with $k_3 = 2k_2$. On the other hand, from (27), (29), and (67) one obtains

$$\begin{aligned} \dot{\xi}_1(t) - 1 &= -a \sum_{j \in J_1} (\xi_1(t) - \xi_j(t)) + e'_{v,1}(t) \\ \dot{\xi}_i(t) - 1 &= -a \sum_{j \in J_i} (\xi_i(t) - \xi_j(t)) + \zeta_{2,i-1}(t) + e'_{v,i}(t), \qquad i = 2, \ldots, n \, , \end{aligned}$$

which, along with the bound in (31) and the fact that $|e'_{v,i}(t)| \leq \frac{|e_{v,i}(t)|}{v_{\min}}$, lead to the bound in (33) with $k_4 = (2a\,(n-1)+1)\,k_2 + \frac{1}{v_{\min}}$. □

E. Proof of Theorem 1

First, in order to simplify the notation in this proof, we define the positive constants $v_{c\,\min}$ and $v_{c\,\max}$ as $v_{c\,\min} \triangleq v_{\min} + \gamma_v$ and $v_{c\,\max} \triangleq v_{\max} - \gamma_v$, which —as shown later in the proof— will characterize the lower and upper bounds on the UAV speed commands. Similarly, let $v_{d,i\,\min}$ and $v_{d,i\,\max}$ be lower and upper bounds on the desired speed profile for the ith UAV, $v_{d,i}(\cdot)$, that is, $v_{d,i\,\min} \leq v_{d,i} \leq v_{d,i\,\max}$, and define $v_{d\,\min}$ and $v_{d\,\max}$ as

$$v_{d\,\min} \triangleq \min_{i \in \{1,\ldots,n\}} v_{d,i\,\min} \, ,$$

$$v_{d\,\max} \triangleq \max_{i \in \{1,\ldots,n\}} v_{d,i\,\max} \, .$$

We note that the assumptions on the initial conditions in (40) and (41) imply that the following bounds hold at time $t = 0$ for all vehicles:

$$v_{c\,\min} \leq v_{c,j}(0) \leq v_{c\,\max} \, , \qquad \forall \; j \in \{1, \ldots, n\} \, .$$

In fact, from the assumption on the initial path-following errors in (40), it follows that, for all $j \in \{1, \ldots, n\}$,

$$\|p_{F,j}(0)\| \leq cc_1 \,, \tag{68}$$

$$\Psi(\tilde{R}_j(0)) \leq c^2 \,. \tag{69}$$

Also, from the proof of Lemma 1, we have that

$$\vec{w}_{1,j} \cdot \vec{b}_{1D,j} = 1 - 2\Psi(\tilde{R}_j) \,,$$

and therefore it follows from (69) that

$$\vec{w}_{1,j}(0) \cdot \vec{b}_{1D,j}(0) \geq 1 - 2c^2 > 0 \,.$$

This inequality, together with the definition of $\vec{b}_{1D,j}$ in (2) and the bound in (68), implies that

$$\vec{w}_{1,j}(0) \cdot \vec{t}_j(0) \geq \frac{d(1-2c^2) - 2c_1c^2(1-c^2)^{\frac{1}{2}}}{(d^2 + c^2c_1^2)^{\frac{1}{2}}} \,.$$

From the choice for the characterizing distance d in (35), it follows that

$$d(1-2c^2) - 2c_1c^2(1-c^2)^{\frac{1}{2}} > 0 \,,$$

and therefore, we have

$$\vec{w}_{1,j}(0) \cdot \vec{t}_j(0) \geq \underbrace{\frac{d(1-2c^2) - 2c_1c^2(1-c^2)^{\frac{1}{2}}}{(d^2 + c^2c_1^2)^{\frac{1}{2}}}}_{\triangleq c_2} > 0 \,, \tag{70}$$

which implies that the quantity $\frac{1}{\vec{w}_{1,j}(0) \cdot \vec{t}_j(0)}$ is thus well defined. From this fact, the definition of the speed commands in (26), the coordination law in (28), the equalities in (65)-(66), and the bounds in (68) and (70), it follows that the speed command at time $t = 0$, $v_{c,j}(0)$, satisfies

$$v_{d,i\,\min} - 2a(n-1)v_{d,i\,\max}\|\zeta(0)\| - K_\ell cc_1 \leq v_{c,j}(0) \leq \frac{1}{c_2}\left(v_{d,i\,\max} + 2a(n-1)v_{d,i\,\max}\|\zeta(0)\| + K_\ell cc_1\right) \,,$$

Then, the assumption on the initial condition in (41) implies that, for all $j \in \{1, \ldots, n\}$,

$$v_{c\,\min} \leq v_{c,j}(0) \leq v_{c\,\max} \,.$$

With this preliminary result in mind, we now prove the claims of the theorem by contradiction. To this effect, we consider one of the UAVs involved in the mission that has not yet reached its final destination, and assume that it violates the results of the theorem, that is, either it is not able to remain inside the prespecified tube centered on its desired path, or its speed command goes outside the acceptable feasible range while trying to keep coordination with the other UAVs. Without loss of generality, we assume that this UAV is the first one that violates (at least) one of these conditions, and therefore we suppose that all other vehicles do satisfy the claims of the theorem. In what follows, we establish the validity of the theorem by showing that the hypotheses above imply a contradiction.

Consider the ith UAV and suppose that, at time $t > 0$, it has not yet reached the final destination (that is, $\ell_i'(t) < 1$). Assume that, at this same time instant t, either the path-following errors of the ith UAV are such that $(p_{F,i}(t), \tilde{R}_i(t)) \notin \Omega_c$, or its speed command $v_{c,i}(t)$ does not satisfy the bounds $v_{c\,\min} \leq v_{c,i}(t) \leq v_{c\,\max}$ (or both). For all other UAVs, we assume that $(p_{F,j}(\tau), \tilde{R}_j(\tau)) \in \Omega_c$ and $v_{c\,\min} \leq v_{c,j}(\tau) \leq v_{c\,\max}$, $j \in \{1, \ldots, n\}$, $j \neq i$, and for all $\tau \in [0, t]$.

Consider first the case in which $(p_{F,i}(t), \tilde{R}_i(t)) \notin \Omega_c$, while $v_{c\,\min} \leq v_{c,i}(\tau) \leq v_{c\,\max}$ for all $\tau \in [0, t]$. For the ith UAV, consider the same path-following Lyapunov function candidate as in the proof of Lemma 1:

$$V_{pf,i}(p_{F,i}, \tilde{R}_i) = \Psi(\tilde{R}_i) + \frac{1}{c_1^2}\|p_{F,i}\|^2 \,.$$

Since $(p_{F,i}(0), \tilde{R}_i(0)) \in \Omega_c$ by assumption, and $V_{pf,i}$ evaluated along the system trajectories is continuous and differentiable, we have that, if $(p_{F,i}(t), \tilde{R}_i(t)) \notin \Omega_c$ for some $t > 0$, then there exists a time t' $(0 \leq t' < t)$ such that

$$V_{pf,i}(t') = c^2 \,, \tag{71}$$

$$\dot{V}_{pf,i}(t') > 0 \,, \tag{72}$$

while

$$V_{pf,i}(\tau) \leq c^2 \,, \qquad \forall\, \tau \in [0, t') \,. \tag{73}$$

The equality in (71) and the bound in (73) imply that the following inequalities hold for all $\tau \in [0, t']$:

$$\|p_{F,i}(\tau)\| \leq cc_1\,, \qquad \Psi(\tilde{R}_i(\tau)) \leq c^2\,,$$

which, along with the choice for the characterizing distance d in (35), imply that

$$\vec{w}_{1,i}(\tau) \cdot \vec{t}_i(\tau) \geq c_2 > 0\,, \qquad \forall\, \tau \in [0, t']\,,$$

where c_2 was defined in (70). The quantity $\frac{1}{\vec{w}_{1,i}(\tau)\cdot\vec{t}_i(\tau)}$ is thus well defined for all $\tau \in [0, t']$, which implies that the speed command $v_{c,i}(\tau)$ in (26) is also well defined for all $\tau \in [0, t']$. Since $v_{\min} < v_{c\,\min} \leq v_{c,i}(\tau) \leq v_{c\,\max} < v_{\max}$ for all $\tau \in [0, t']$ by hypothesis, the assumption on the UAV dynamics in (13) implies that

$$|v_{c,i}(\tau) - v_i(\tau)| \leq \gamma_v\,, \qquad \forall\, \tau \in [0, t']\,.$$

Then, it follows that

$$v_{\min} \leq v_i(\tau) \leq v_{\max}\,, \qquad \forall\, \tau \in [0, t']\,.$$

We can now use a proof similar to the one of Lemma 2 to show that, for all $\tau \in [0, t']$, $\dot{V}_{pf,i} < 0$ on the boundary of Ω_c, which contradicts the claim in (71)-(72).

Next, we consider the case in which the bounds $v_{c\,\min} \leq v_{c,i}(t) \leq v_{c\,\max}$ do not hold, while $(p_{F,i}(\tau), \tilde{R}_i(\tau)) \in \Omega_c$ for all $\tau \in [0, t]$. Let t' $(0 < t' \leq t)$ be the first time at which $v_{c\,\min} \leq v_{c,i} \leq v_{c\,\max}$ is not satisfied. Then, we have that at time t' one of the following bounds holds:

$$v_{c\,\min} > v_{c,i}(t')\,, \qquad \text{or} \qquad v_{c,i}(t') > v_{c\,\max}\,, \tag{74}$$

while

$$v_{c\,\min} \leq v_{c,i}(\tau) \leq v_{c\,\max}\,, \qquad \forall\, \tau \in [0, t')\,. \tag{75}$$

Since $(p_{F,i}(\tau), \tilde{R}_i(\tau)) \in \Omega_c$ for all $\tau \in [0, t']$ by hypothesis, the following bounds hold for all $\tau \in [0, t']$:

$$\|p_{F,i}(\tau)\| \leq cc_1\,, \tag{76}$$

$$\Psi(\tilde{R}_i(\tau)) \leq c^2\,, \tag{77}$$

which, along with the choice for the characterizing distance d in (35), imply that

$$\vec{w}_{1,i}(\tau) \cdot \vec{t}_i(\tau) \geq c_2 > 0\,, \qquad \forall\, \tau \in [0, t']\,. \tag{78}$$

The bound in (75), along with the assumption on the UAV dynamics in (13), imply that

$$|v_{c,i}(\tau) - v_i(\tau)| \leq \gamma_v\,, \qquad \forall\, \tau \in [0, t')\,, \tag{79}$$

which, in turn, leads to

$$v_{\min} \leq v_i(\tau) \leq v_{\max}\,, \qquad \forall\, \tau \in [0, t')\,.$$

Continuity of v_i and the bound above imply that $v_i(t')$ is bounded, and therefore $\ell_i'(\tau)$ is continuous and stays bounded for all $\tau \in [0, t']$. Since we have assumed that the ith UAV has not yet reached its final destination at time t, we also have that $\ell_i'(t') < 1$. Then, from the definition of the coordination states in (9), it follows that $\xi_i(\tau)$ is also continuous and bounded for all $\tau \in [0, t']$. Moreover, since (by hypothesis) the bounds $v_{c\,\min} \leq v_{c,j}(\tau) \leq v_{c\,\max}$ hold for all $j \in \{1, \ldots, n\}$, $j \neq i$, and for all $\tau \in [0, t']$, it follows from the assumption on the UAV dynamics in (13) that

$$|v_{c,j}(\tau) - v_j(\tau)| \leq \gamma_v\,, \qquad \forall\, j \in \{1, \ldots, n\}\,;\ j \neq i\,, \qquad \forall\, \tau \in [0, t']\,, \tag{80}$$

which leads to

$$v_{\min} \leq v_j(\tau) \leq v_{\max}\,, \qquad \forall\, j \in \{1, \ldots, n\}\,;\ j \neq i\,, \qquad \forall\, \tau \in [0, t']\,.$$

This bound, along with the hypothesis that $(p_{F,j}(\tau), \tilde{R}_j(\tau)) \in \Omega_c$ for all $j \in \{1, \ldots, n\}$, $j \neq i$, and for all $\tau \in [0, t']$, implies that $\xi_j(\tau)$ is bounded for all $j \in \{1, \ldots, n\}$, $j \neq i$, and for all $\tau \in [0, t']$. Boundedness of $\xi_j(\tau)$ for all $j \in \{1, \ldots, n\}$ and for all $\tau \in [0, t']$ implies that $u_{\text{coord},i}(t')$ is bounded, which, together with the inequality in (78), implies that $v_{c,i}(t')$ is also bounded. Hence, we can conclude that $e_{v,i}(t')$ is bounded. Then, since the speed tracking error vector $e_v(\tau)$ is bounded for all $\tau \in [0, t']$, a proof similar to the one of Lemma 3 can be used to show that the choice of the coordination control gains a and b in (37) ensures that there exists a positive constant λ_c such that

$$\|\zeta(\tau)\| \leq k_1 \|\zeta(0)\| \mathrm{e}^{-\lambda_c \tau} + k_2 \sup_{s \in [0, \tau)} \|e_v(s)\|\,, \qquad \forall\, \tau \in [0, t']\,,$$

and hence, the bounds on the speed tracking errors in (79) and (80) lead to

$$\|\zeta(t')\| \leq k_1 \|\zeta(0)\| + k_2 \sqrt{n}\, \gamma_v\,.$$

From the inequality above, the speed command in (26), the coordination law in (28), the equalities in (65)-(66), and the bounds in (76) and (78), it follows that the speed command at time t', $v_{c,i}(t')$, satisfies

$$v_{d,i\,\min} - v_{d,i\,\max}\left(\bar{k}_1\|\zeta(0)\| + \bar{k}_2\sqrt{n}\,\gamma_v\right) - K_\ell cc_1 \leq v_{c,i}(t') \leq \frac{1}{c_2}\left(v_{d,i\,\max} + v_{d,i\,\max}\left(\bar{k}_1\|\zeta(0)\| + \bar{k}_2\sqrt{n}\,\gamma_v\right) + K_\ell cc_1\right),$$

where $\bar{k}_1$ and $\bar{k}_2$ were introduced in (41) and (39) respectively. The assumption on the initial condition in (41) implies that

$$v_{\min} + \gamma_v \leq v_{c,i}(t') \leq v_{\max} - \gamma_v\,,$$

which contradicts the claim in (74).

Finally, similar arguments can be used to prove the impossibility of both $(p_{F,i}, \tilde{R}_i) \in \Omega_c$ and $v_{c\,\min} \leq v_{c,i} \leq v_{c\,\max}$ failing to hold at the exact same time.

Therefore, we have that, for all $i \in \{1, \ldots, n\}$ and for all $t \geq 0$, the path-following errors $p_{F,i}(t)$ and $\tilde{R}_i(t)$ satisfy

$$(p_{F,i}(t), \tilde{R}_i(t)) \in \Omega_c\,,$$

while the speed command $v_{c,i}(t)$ verifies the bounds

$$v_{c\,\min} \leq v_{c,i}(t) \leq v_{c\,\max}\,. \tag{81}$$

It follows from the bound in (81) and the assumption on the UAV dynamics in (13) that

$$|v_{c,i}(t) - v_i(t)| \leq \gamma_v\,, \qquad \forall\, i \in \{1, \ldots, n\}\,, \qquad \forall\, t \geq 0\,,$$

which leads to

$$v_{\min} \leq v_i(\tau) \leq v_{\max}\,, \qquad \forall\, i \in \{1, \ldots, n\}\,, \qquad \forall\, t \geq 0\,.$$

Moreover, the choice for the characterizing distance d in (35) implies that

$$\vec{w}_{1,i}(\tau) \cdot \vec{t}_i(\tau) \geq c_2 > 0\,, \qquad \forall\, i \in \{1, \ldots, n\}\,, \qquad \forall\, t \geq 0\,.$$

Then, the bounds in (42)-(43) and (44) follow respectively from proofs similar to those of Lemmas 2 and 3. □